buildings

MDPI

Article

Experimental and Numerical Investigation of Historic Brickwork Masonry with Weak and Degraded Joints: Failure Mechanisms Under Compression and Shear

Erica Magagnini *, Vanni Nicoletti and Fabrizio Gara

Department of Construction, Civil Engineering and Architecture (DICEA), Università Politecnica delle Marche, Via Brecce Bianche 12, 60131 Ancona, Italy; v.nicoletti@univpm.it (V.N.); f.gara@univpm.it (F.G.)
* Correspondence: e.magagnini@univpm.it

Abstract

The failure behaviour of historic unreinforced masonry (URM) structures is strongly influenced by the properties of bricks and mortar. Over time, degradation processes compromise these materials, with significant effect on structural response and safety. Nevertheless, deterioration effects on the nonlinear behaviour of masonry have been only marginally investigated. This study investigates the mechanical behaviour and failure mechanisms of historic brick masonry with weak and irregular mortar joints, representative of Mediterranean traditional constructions. An extensive experimental programme was conducted on mortars, historic clay bricks, prisms, wallets, and triplet specimens, complemented by in-situ flat jack tests. Results confirm the critical role of mortar quality and joint irregularities in reducing compressive and shear strength and in influencing deformation capacity of historic masonry. The experimental findings served as a basis for the calibration of a Finite Element Model (FEM), subsequently employed to gain deeper insight into the governing failure mechanisms in a real study case. A critical discussion of compression and shear failure criteria is presented, focusing on historic masonry. Experimental and analytical comparisons show major discrepancies in classical criteria, especially with degraded mortars. The study shows that in historic masonry with weak joints, failure is often governed by compression rather than shear.

Keywords: historic brickwork masonry; weak mortar joints; experimental testing; failure mechanisms; compression loading; shear behaviour; earthquake; FEM

Academic Editor: Nerio Tullini

Received: 6 October 2025
Revised: 30 October 2025
Accepted: 2 November 2025
Published: 5 November 2025

Citation: Magagnini, E.; Nicoletti, V.; Gara, F. Experimental and Numerical Investigation of Historic Brickwork Masonry with Weak and Degraded Joints: Failure Mechanisms Under Compression and Shear. *Buildings* **2025**, *15*, 3993. https://doi.org/10.3390/buildings15213993

1. Introduction

Masonry buildings represent a substantial and invaluable component of the global built heritage. Across many European and Mediterranean countries exposed to moderate-to-high seismic hazard—such as Italy, Greece, Slovenia, Albania, Morocco, and Turkey—unreinforced masonry (URM) structures constitute the majority of the historic building stock, making their seismic vulnerability a critical concern [1].

Masonry can be considered a highly complex construction material, both with regard to its mechanical properties and its behaviour under different loading conditions. The heterogeneous composition of masonry represents a primary challenge, as its mechanical response generally derives from the interaction between mortar joints and masonry units. The structural performance of masonry thus depends not only on the mechanical

characteristics of its individual constituents, but also on the bonding pattern, namely the arrangement and interconnection of units [2]. The significant variability in the properties of both materials and assemblages makes the tasks of structural modelling, analysis, and safety verification particularly demanding. The variability of masonry properties cannot be attributed solely to intrinsic factors such as bond pattern, type of units, and the presence of mortar joints. Equally significant are extrinsic influences, including the quality of workmanship during construction and the environmental conditions to which the structure is exposed throughout its service life (e.g., high moisture content, thermal cycles, and the presence of salts) [3,4]. These factors may induce progressive changes in the material properties, thereby compromising the structural performance and amplifying the extent of damage in the event of hazardous actions such as earthquakes, landslides, floods, or impacts [5–8].

The assessment of mechanical behaviour and load-bearing capacity of historic masonry constitutes the essential premise for any diagnostic process of masonry structures. Preventive and rehabilitative interventions can be effectively undertaken only when the actual condition of the structure is clearly identified, and the possible failure mechanisms are carefully defined. Furthermore, the proper management of a restoration project proves unattainable in the absence of reliable knowledge.

A large part of the existing literature on the assessment of the structural behaviour and safety of masonry constructions concentrates on their response to seismic actions [9]. Historic URM buildings generally exhibit very low mechanical strength when subjected to seismic actions, resulting in an inadequate structural response. Partial collapses, or in more severe cases the complete failure of entire masonry structures, are primarily attributable to the poor mechanical properties of the constituent materials, which often lack adequate compressive strength and exhibit negligible shear resistance [10]. Recent post-earthquake reconnaissance studies have further confirmed the high seismic vulnerability of unreinforced masonry (URM) buildings in regions of moderate to high seismic hazard. Field observations following the 2023 Kahramanmaraş (Türkiye) earthquakes revealed extensive damage and collapse of historic and vernacular masonry constructions, mainly associated with low tensile strength, poor mortar–unit interaction, poor connection between orthogonal walls, inadequate wall continuity and weak joint response [11,12]. These findings are consistent with earlier observations from Mediterranean seismic events [13,14], emphasizing that the interaction of material degradation (e.g., weak or deteriorated mortar joints), construction irregularities and seismic action play a controlling role in failure mechanisms of historic masonry. By explicitly recognising these recent field observations, the need for a detailed mechanical characterisation of historic brickwork—as addressed in the present work—becomes even more compelling. Furthermore, 2016–2017 Central Italy seismic events (Amatrice–Norcia–Visso sequence) revealed that, in addition to horizontal accelerations, significant vertical components further increased the fragility of low-cohesion masonry [15]. The resulting damage, often in the form of vertical cracking, highlights that failure mechanisms in such structures may be predominantly governed by compression. In addition to seismic action, historic masonry buildings may experience significant damage and, subsequently, even failure, due to a variety of other causes, often concurrent and cumulative. These include excessive or unevenly gravitational loads; foundation soil settlements and movements [16,17]; environmental actions and material degradation [18]; thermal actions and hygrometric variations [19]; exceptional or accidental actions [20]; as well as construction errors or subsequent modifications.

Over recent decades, modern brickwork has been the subject of extensive and systematic investigations, with numerous contributions addressing the experimental behaviour of masonry walls under compression [21,22] and shear [23–26]. Based on these

results, various authors have proposed failure criteria for masonry [27–29]. This research field has played a crucial role in the formulation of Codes of Practice for civil engineering applications [30–32]. The behaviour of historic brickwork, on the other hand, has been less extensively investigated, both experimentally and theoretically. The majority of the literature concerning the structural behaviour and safety of existing historic masonry structures addresses buildings exposed to seismic hazard, with a predominant focus on the assessment of global seismic performance at the scale of the entire building with numerical simulations—considering both in-plane and out-of-plane mechanisms [33–37]—and on the evaluation of dynamic properties through Structural Health Monitoring strategies [38–40]. To date, research specifically devoted to historic brickwork masonry panels remains insufficient, particularly regarding the characterization of brickwork as a composite system defined by the properties of its individual constituent materials [7,41]. The complexity of the mechanical and geometric factors influencing the strength of historic bricks requires a more comprehensive assessment of their effective response, encompassing shear, tensile, and compression behaviour. Despite the extensive literature on modern masonry and on the global seismic assessment of historic buildings, there remains a significant knowledge gap regarding the mechanical characterization of degraded historic masonry at the material and sub-structural scale. The influence of weak, irregular, and deteriorated mortar joints—commonly found in historic constructions—on the compression and shear behaviour as well as on the associated failure mechanisms of brick masonry, remains insufficiently understood. Previous studies often rely on formulations developed for modern, regular masonry, which tend to overestimate the strength and stiffness of historic fabric.

The present work investigates the mechanical behaviour of historic masonry through the analysis of its response under pure compression and combined compression–shear loading conditions. The failure mechanisms of historic brickwork are analysed by experimental laboratory tests on solid bricks, mortar and wallets built using historic full-scale bricks and one-third-scale clay specimens, together with in-situ flat jack-tests. The experimental programme was carried out on masonry specimens composed of historic bricks and mortars, carefully selected to reproduce the mechanical characteristics of the traditional construction techniques typical of existing buildings in Southern Europe. Investigation has been developed considering clay units from two monumental churches located in Central Italy and damaged by seismic events of 2016–2017: Santa Maria Ausiliatrice Church in Montottone (FM) and San Pietro Church in Corridonia (MC) (Figure 1a–c). In addition, the Church of Santa Maria Ausiliatrice, over the years subjected to various forms of damage primarily of seismic origin, was selected as a case study for performing a Finite Element Modelling (FEM) analysis, carefully calibrated using the results of experimental tests, in order to evaluate the main mechanisms that may lead to failure in a real damaged structure.

Finally, failure mechanisms under compression and shear loading are discussed to describe the actual behaviour of brickwork and to assess their applicability to historic masonry with irregular and degraded mortar joints. Indeed, one of the aims of this paper is also to understand whether the failure criteria available for modern masonry may be suitable for verifying safety of masonry buildings in seismic regions, in presence of intrinsic weakness of construction materials and deteriorated mortar joints. The outcomes provide new insight into the governing role of weak mortar joints, the limitations of classical failure criteria, and the prevalence of compression-related failure mechanisms in historic masonry.

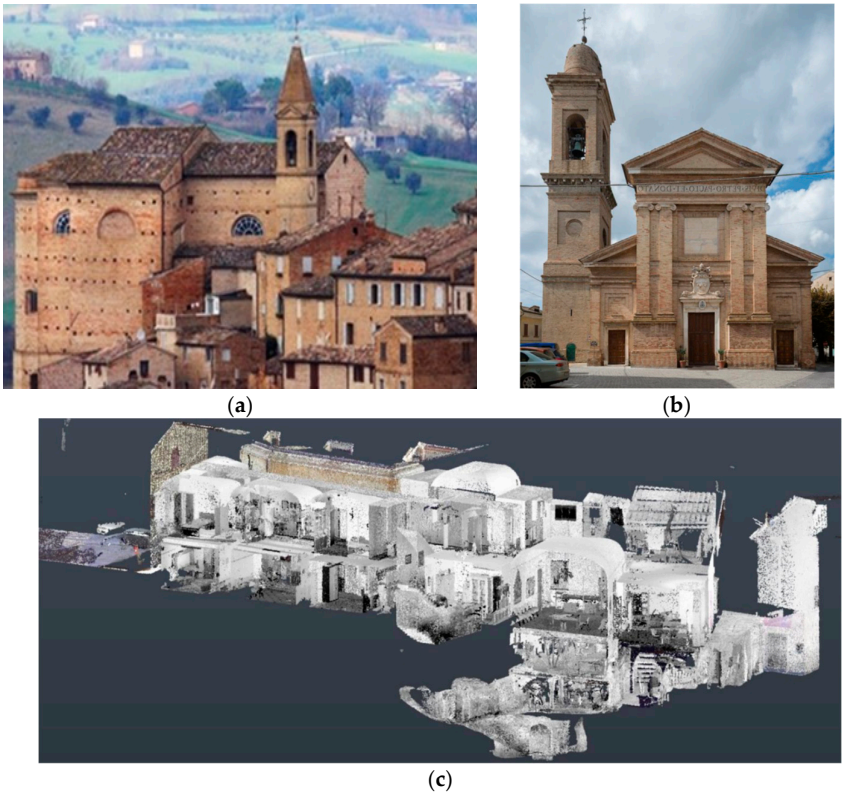

Figure 1. (**a**) View of the church of Santa Maria Ausiliatrice in Montottone (FM); (**b**) church of San Pietro in Corridonia (MC); (**c**) laser scanning of the building complex of the San Pietro church.

The novelty of this research lies in providing an integrated experimental–numerical–analytical framework to investigate the actual mechanical response of historic brick masonry, combining laboratory tests on historic materials, in-situ flat-jack tests, and finite element simulations on real case studies. This approach allows the identification of specific failure modes and corrective parameters applicable to degraded, low-strength masonry, thereby improving the reliability of structural assessments and supporting the development of more accurate and conservative verification criteria for the preservation of historic buildings.

2. Experimental Methodology

The analysis of masonry failure mechanisms usually refers to modern masonry with good-quality bricks, with adequate compressive and tensile strength, and regular arrangement with relatively thin mortar joints. Historic masonry, on the other hand, is characterized by bricks of lower strength and variable in both state of preservation and different construction techniques. Another aspect to consider is that historic masonry is often characterized by poor quality mortars based on lime as the main binder, whose mechanical properties may undergo severe degradation over time due to processes such as leaching, freeze–thaw cycles, salt crystallization, and long-term environmental ageing in service [7]. In historic masonry buildings, there is also considerable variability in the dimensions of mortar joints from one point of the structure to another, often reaching substantial dimensions.

The accurate identification of mechanical parameters is essential to ensure high reliability in modelling outcomes. For new masonry constructions, the Italian Technical Code [29,30], in alignment with Eurocode 6 [32], allows the estimation of compressive and shear strength either through predefined tabulated values based on the properties of the

constituent materials or by means of experimental tests conducted in accordance with the EN 1052-1 standard [42] and EN 1052-3 [43]. Conversely, in the case of existing masonry structures, experimental data collected for the most common masonry types have been processed to provide typical ranges of average compressive strength and elastic moduli, see chapter 8 of Italian Technical Code [30]. These values are presented in tabular form and can be adjusted to reflect the actual condition of the masonry and any previous strengthening interventions. Nevertheless, experimental testing is strongly recommended to achieve an appropriate level of knowledge of existing structures.

Based on such considerations, the experimental programme presented in this paper has been carried out on mortars, historic clay bricks, and masonry elements, with the aim of obtaining the main parameters that affect the failure behaviour of masonry. Experimental tests were conducted on historic masonry by taking clay bricks from the existing historic buildings described in the Introduction and reproducing the characteristics of the mortars in laboratory. The historic bricks were collected exclusively from the internal walls of two churches located in Corridonia (Macerata) and Montottone (Fermo), Central Italy. Both sites have a humid temperate climate, with average annual temperatures of 13–14 °C. Although the internal bricks were protected from direct exposure to rain and temperature extremes, they were influenced by indoor microclimatic variations typical of historic unheated buildings. The churches date back to the late 18th–early 19th century, and the bricks are estimated to be around 200 years old. The choice of materials was guided by the objective of replicating conditions that are representative of historical masonry structures.

The investigation was developed at the "Giovanni Menditto" Materials and Structures Testing Laboratory of the Polytechnic University of Marche. Figure 2 summarizes the testing configuration of the entire experimental campaign. Tables 1–3 provide a concise overview of the experimental programme, including number of specimens, sample size and specimen dimensions. The adopted number of specimens per test category reflects a compromise between experimental significance and the limited recoverable quantity of historic materials. The consistency of the results has been assessed through the coefficient of variation (CoV), thereby ensuring a transparent evaluation of dataset quality and representativeness.

Table 4 summarizes the test typologies and the mechanical parameters obtained, together with the relevant standard specifications for the characterization of mortar, brick, and historic masonry.

Table 1. Testing on mortar samples: number of specimens (No.), specimen dimensions and experimental test type.

Specimen	No.	Test Type	Name	Dimensions [mm]		
				a	b	t
A	2	Bending tests—Figure 2a	$M_{A,BENDING}$	160	40	40
1:1:5	4	Compression tests—Figure 2b	$M_{A,COMPRESSION.}$	40	40	40
cement:lime:sand	1	Compression tests—Figure 2c	$M_{A,COMPR.\ PRISMS}$	40	160	40
B	2	Bending tests—Figure 2a	$M_{B,BENDING}$	160	40	40
1:3	4	Compression tests—Figure 2b	$M_{B,COMPRESSION}$	40	40	40
lime:sand	1	Compression tests—Figure 2c	$M_{B,COMPR.\ PRISMS}$	40	160	40

Table 2. Testing on historic bricks: number of specimens (No.), specimen dimensions and experimental test type.

No.	Test Type	Name	Dimensions [mm]		
			a	b	t
11	Splitting test—Figure 2d	B1	100	100	53
		B2	100	100	57
		B3	100	100	55
	Compression perpendicular to the bed faces—Figure 2e	B4	296	55	147
		B5	283	50	155
	Compression parallel to the bed faces—Figure 2f	B6	148	311	50
		B7	137	280	44
	Compression parallel to the head face—Figure 2g	B8	240	110	50
		B9	240	110	50
	Compression on prisms Figure 2h	B10	40	100	20
		B11	40	100	20

Table 3. Testing on masonry samples: specimen dimensions and experimental test type.

No.	Test Type	Name	Dimensions [mm]		
			a	b	t
8	Uniaxial compression on prisms Figure 2i	P1	268	300	150
		P2	268	310	155
		P3	293	300	150
		P4	275	305	120
		P5	270	305	122
	Uniaxial compression on wallettes Figure 2j	W1	350	580	130
		W2	350	580	130
		W3	540	580	350
3	Diagonal compression on wallettes Figure 2k	S1	699	864	130
		S2	680	830	130
		S3	685	833	130
11	Triplet tests Figure 2l Type T mortar 1:1:5 (cement:lime:sand) Type R mortar 1:3 (lime:sand) Y = yellow bricks R = red bricks	T1 (Y)	100	61	25
		T2 (R)	100	61	25
		T3 (Y)	100	61	25
		T4 (R)	100	61	25
		T5 (Y)	100	61	25
		T6 (R)	100	61	25
		R1 (R)	100	61	25
		R2 (Y)	100	61	25
		R3 (R)	100	61	25
		R4 (Y)	100	61	25
		R5 (R)	100	61	25

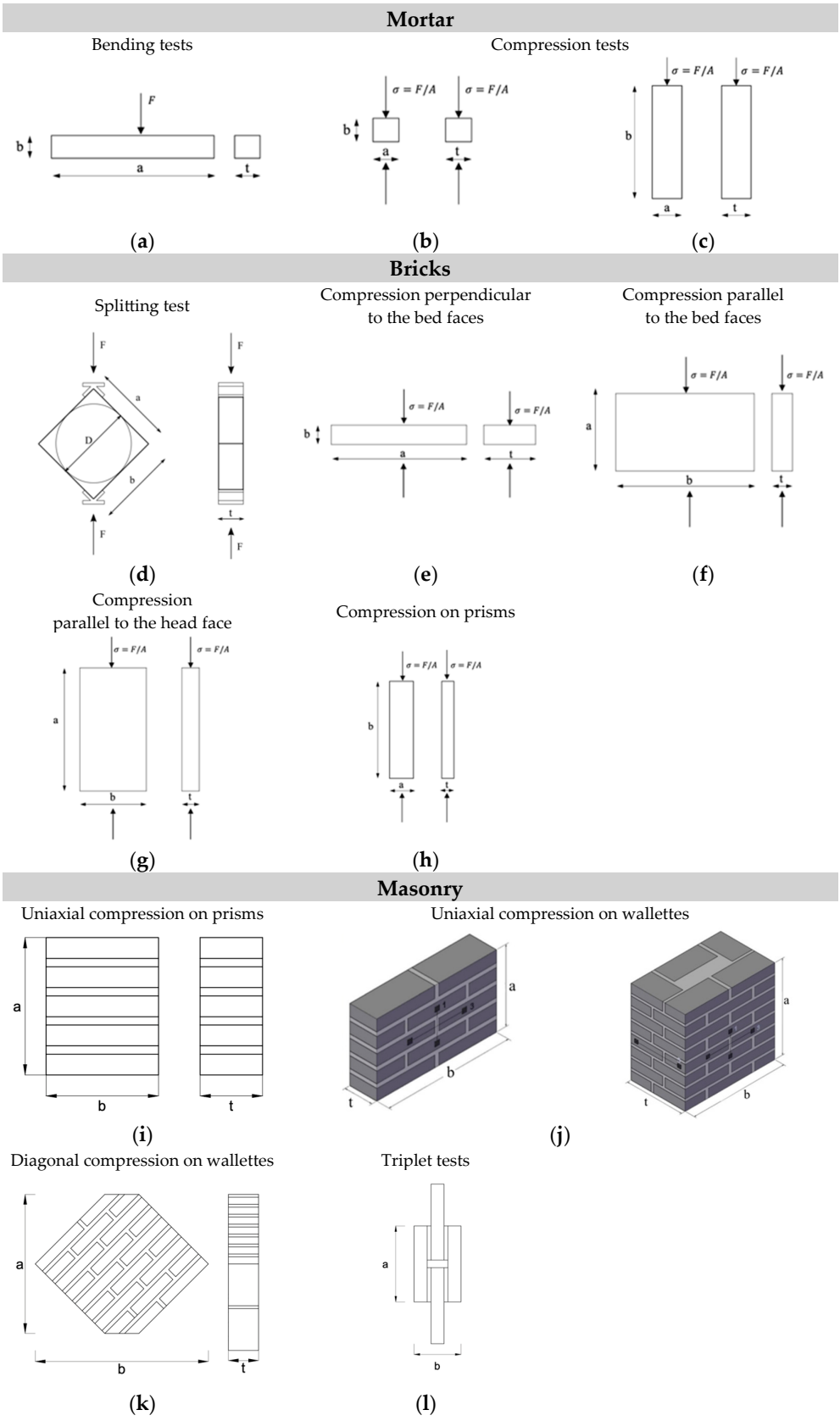

Figure 2. Configurations of experimental laboratory tests: (**a**) bending tests on mortar, (**b**) compression tests on mortar cubes, (**c**) compression test on mortar prims, (**d**) splitting test on bricks, (**e**) compression tests perpendicular to the brick's bed faces, (**f**) compression tests parallel to the

brick's bed faces, (**g**) compression tests parallel to the brick's head faces, (**h**) compression on brick's prisms, (**i**) uniaxial compression tests on prisms, (**j**) uniaxial compression tests on wallettes, (**k**) diagonal compression on wallettes and (**l**) triplet tests.

Table 4. Experimental campaign: mechanical parameters and standard specifications for mortar, brick, and masonry.

Specimen	Test Type	Mechanical Parameters	Standards
Mortar	Bending test	Tensile strength (f_{tm})	EN 1015-11
	Compression test	Compressive strength (f_m)	
		Compressive Young's modulus (E_m)	EN 1926
		Poisson's coefficient (ν_m)	
Brick	Splitting test	Tensile strength (f_{tb})	EN 12390-6
	Compression test	Compressive strength (f_b)	EN 1015-11
		Compressive Young's modulus (E_b)	EN 1926
		Poisson's coefficient (ν_b)	
Masonry	Compression test	Compressive strength (f_w)	EN 1052-1
	Diagonal compression test	Compressive Young's modulus (E_w)	
		Poisson's coefficient (ν_w)	
		Tensile strength (f_{tw})	EN 1052-3
	Triplet test	Shear strength (τ_0)	RILEM TC 127-MS

2.1. Experimental Test on Mortars and Bricks

The first part of the experimental programme involves the characterization of mortar and bricks that are the key components of the masonry system.

Regarding mortar, the composition was designed according to formulations and mix designs widely reported in the scientific literature for conservation of cultural heritage structures [44–46]. Specifically, the selected binder–aggregate ratios and the type of lime were chosen to reproduce the physical and mechanical behaviour typically observed in traditional historic mortars—namely low mechanical strength, high vapor permeability, and compatible elastic modulus with the historic masonry units.

As indicated in Table 1, two different typologies of mortars have been investigated. The first typology consists of a cementitious mortar with a cement/lime/sand ratio by volume equal to 1:1:5 (Type A). The second one is a natural hydraulic lime (NHL) mortar with fine sand, having a binder-to-aggregate ratio of 1:3 by volume (Type B). The mortar compositions were specifically designed to simulate different conditions commonly observed in historic masonry (Table 5). A mix ratio of 1:1:5 was adopted to reproduce a low-strength mortar in a well-preserved state, whereas a mix ratio of 1:3 was selected to represent a weak mortar in poor maintenance conditions. The curing procedure of the specimens involved a temperature of 20 °C (±1 °C) and a relative humidity of 65% (±8%) until testing.

Table 5. Composition summary of the mortars prepared.

Mortar Types	Aggregate	Binder	Binder: Aggregate Ratios (by Volume)	Water: Binder Ratios
Type A	Siliceous sand (grain size 0–0.6 mm)	Portland Cement CEMII 32.5 R Hydraulic lime CL-90 S	1:1:5	0.50
Type B	Siliceous sand (grain size 0–0.6 mm)	Natural hydraulic lime NHL 2	1:3	0.55

Flexural and compressive tests, respectively, on prismatic and cubic mortar specimens have been carried out (Figure 3a,b). In addition, compression tests were carried out on prismatic specimens for the determination of the Young's modulus, E_m, and the Poisson's coefficient, ν_m, for each type of mortar (Figure 3c). Two strain gauges were arranged for each specimen, one for compressive strain and the other for lateral deformation. The experimental results obtained are summarized in Table 6. These results are consistent with findings reported in the literature [47], which indicate compressive strength values below 1.5 MPa for lime mortars typically used in historic structures.

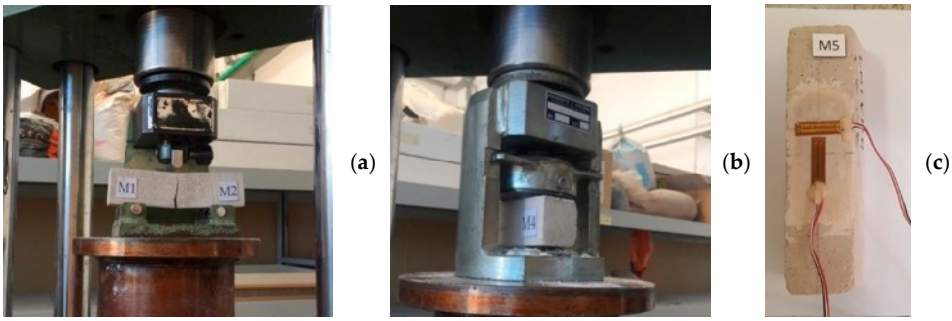

(**a**) (**b**) (**c**)

Figure 3. Mortar specimen testing: (**a**) bending tensile test; (**b**) compression test on cubes, (**c**) example of strain gauges arrangement in prisms.

Table 6. Experimental results on mortar specimens (coefficient of variation in brackets).

Mortar Type	Tensile Strength f_{tm} [N/mm²]		Compressive Strength f_m [N/mm²]		Young's Modulus E_m [N/mm²]	Poisson's Coefficient ν_m
	Min ÷ Max	Average	Min ÷ Max	Average		
$M_{A\ 1:1:5}$	1.73 ÷ 1.85	1.79 (4.75%)	3.07 ÷ 3.99 [2] 3.42 [3]	3.52 (9.47%)	1003.34	0.19
$M_{B\ 1:3}$	- [1]	- [1]	0.43 ÷ 0.65 [2] 0.33 [3]	0.48 (28.15%)	537.00	0.35

[1] Specimens reached immediately failure; [2] Mortar strength by cube tests; [3] Mortar strength by prism tests.

With regard to clay masonry units, two types of bricks were investigated—yellow and red—mainly distinguished by their firing conditions and the chemical composition of the clay matrix. The chromatic distinction is predominantly governed by iron oxide concentration, whereby higher content promotes the formation of red phases during firing, while lower concentrations result in yellowish hues. A total of five experimental tests were performed (Table 2): splitting tensile tests (Figure 4a) and four different compression tests, in which the compressive load was applied perpendicular (Figure 4b) and parallel to the bed face of the brick (Figure 4c), parallel to the head face (Figure 4d), and on prisms (Figure 4e).

(**a**)

(**b**) (**c**) (**d**) (**e**)

Figure 4. (**a**) Splitting tests on brick specimens and compression tests on brick samples (**b**) B4, B5, (**c**) B6, B7, (**d**) B8, B9, (**e**) B10, B11.

The choice of arranging compression tests along three different directions and on clay prisms was done in light of the high sensitivity and dispersion of the results depending on the test method. For samples tested under compression with the load parallel to the bed face of the brick (B6 and B7, as indicated in Table 2), the evolution of the entire strain pattern has been recorded with a couple of linear variable differential transformer (LVDT) placed at the specimen mid-height (Figure 4c) and the applied force has been measured by means of the machine load cell. A sample failure of handmade bricks under uniaxial compression and splitting tests can be seen in Figure 5. Mechanical parameters obtained from the entire experimental campaign on the historic bricks are shown in Table 7.

Table 7. Experimental mechanical parameters of historic bricks (coefficient of variation in brackets).

	Compressive Strength f_b [N/mm²]				**Tensile Strength $f_{b,t}$ [N/mm²]**	**Young's Modulus E_b [N/mm²]**	**Poisson's Ratio ν_b**
Min. value ÷ max value	24.2 ÷ 31.1 [1]	16.2 ÷ 24.1 [2]	11.2 ÷ 17.7 [3]	17.2 ÷ 18.8 [4]	1.08 ÷ 1.45	2769 ÷ 4602	0.126 ÷ 0.124
Average value	27.65 (17.64%)	20.15 (27.72%)	14.45 (31.79%)	18.00 (6.28%)	1.27 (20.68%)	3685.5 (35.17%)	0.13 (1.13%)

[1] perpendicular to the bed faces; [2] parallel to the bed face; [3] parallel to the head face; [4] on prims.

In Table 7, the Young's modulus was evaluated using the sources of data derived from the LVDT's strain measurements. The Young's modulus was evaluated considering the stress range between 30% and 40% of the maximum stress. Experimental results confirm the vast variability of compressive resistance in the case of solid historic bricks. Table 7 shows that the different test methods resulted in values of strength and ultimate deformation that are not directly comparable. When the compressive load is applied parallel to the bed face, the measured strength is influenced by instability phenomena triggered by the formation of vertical cracks aligned with the loading direction. While the values obtained with the compressive load perpendicular to the bed face are affected by confinement phenomena given by the friction with the plates of the testing machine. From this point of view, compression tests on prisms overcome this results' dependence on test methods.

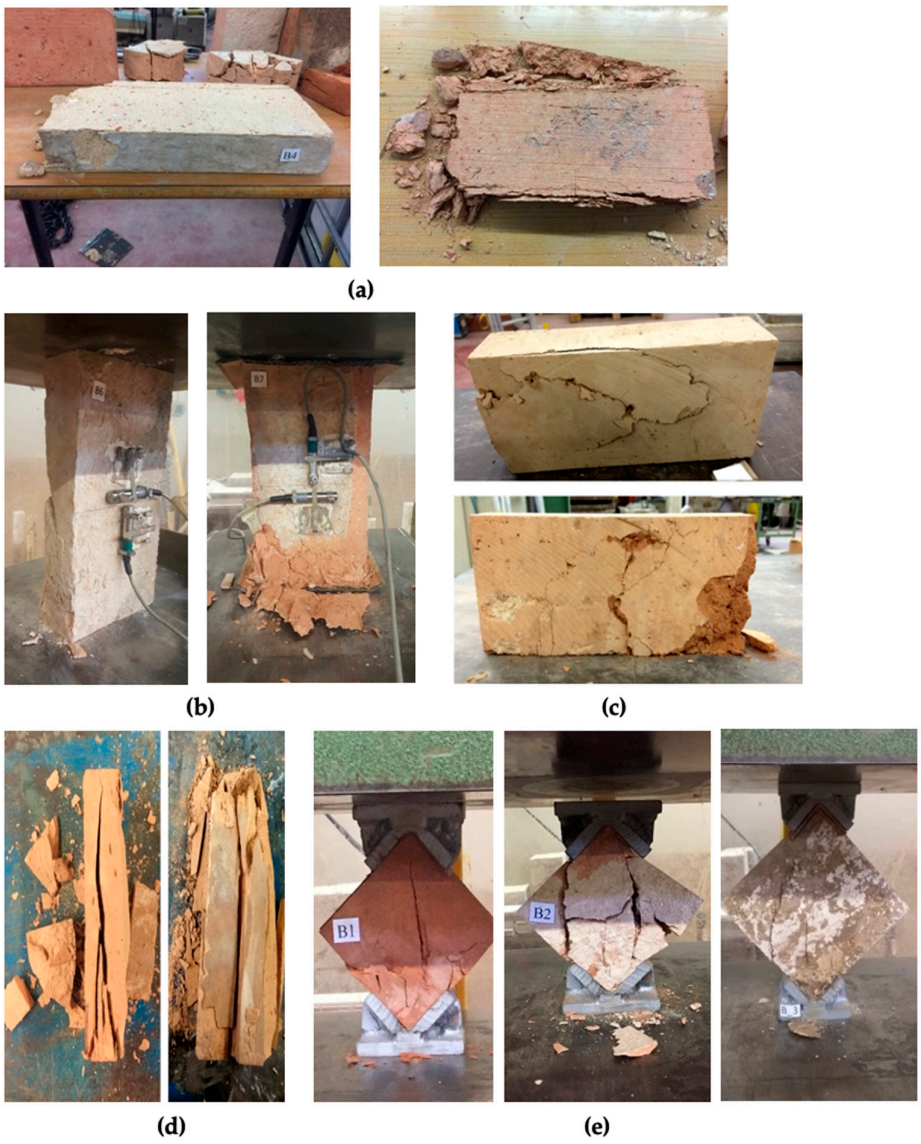

Figure 5. Failure by compression load in brick specimens (**a**) B4 and B5, (**b**) B6 and B7, (**c**) B8 and B9, (**d**) B10 and B11; (**e**) failure by tensile stresses in B1, B2 and B3 brick specimens.

For what concern splitting tests provided in Table 7, the tensile strength of bricks was calculated using the following formula:

$$f_{t,b} = \frac{2 \cdot F}{\pi \cdot D \cdot t} \quad (1)$$

where F is the maximum compressive force obtained at brick failure; D and t are, respectively, the diameter of the circle inscribed inside the brick and the thickness of the brick (Table 2).

2.2. Compression Tests on Prisms and Wallettes

The compression test on masonry was performed following the UNI EN 1052-1 standard [41]. Three uniaxial compression tests were carried out on three prisms P1, P2 and P3 made with historic bricks and 1:1:5 mortar (Figure 6a). In addition, two tests were carried on prisms P4 and P5 with historic bricks and weak mortar joints of lime-sand 1:3 (Figure 6b). The samples were tested 28 days after mortar application. The curing of the specimens was carried out under controlled laboratory conditions (20 ± 1 °C; 65 ± 8% RH)

until the time of testing. Figure 6 shows laboratory test setup with LVDTs mounted on both surfaces for displacement evaluation. Finally, uniaxial compression tests were performed also on single and multi-leaf masonry specimens. Two compression tests were conducted on historic masonry consisting of two wallettes, named W1 and W2, made up of weak mortar joints with a lime-sand ratio of 1:3. Special attention was given to the preparation of the specimens in order to replicate field conditions in the bonding pattern, both regarding the arrangement of the units and their interconnections (Figure 7a). To this end, increased mortar joint thickness, irregular joint geometry, and localized mortar voids were deliberately reproduced (Figure 7b). Beyond the W1 and W2 wallettes, additional tests were conducted on wallette W3, composed of historic bricks in the external leaves and a lime mortar infill (Table 3), specifically designed to reproduce the structural response of multiple-leaf masonry with an intermediate mortar core, a construction typology extensively documented in historic masonry practice. Specimen W3 was built with a 1:3 lime–sand mortar mix applied to both the joints and the central core, and instrumented with LVDTs positioned on each side of the specimens (Figure 7c). Table 8 summarizes the main geometrical properties of masonry prisms and wallettes.

Table 8. Experimental geometric parameters of prisms and wallettes subjected to uniaxial compression tests.

Specimen	Mortar	a [mm]	b [mm]	t [mm]	Average Mortar Joint's Thickness t_m [mm]	Brick's Thickness t_b [mm]	Cross-Section's Area [mm²]
P1	1:1:5	268	300	150	20	40	45,000
P2	1:1:5	268	310	155	21	40	48,050
P3	1:1:5	293	300	150	22	45	45,000
P4	1:3	275	295	120	20	40	35,400
P5	1:3	270	300	122	20	45	36,600
W1	1:3	350	580	130	18	45	75,400
W2	1:3	350	580	130	18	45	75,400
W3	1:3	540	580	350	18	45	203,000

(**a**)

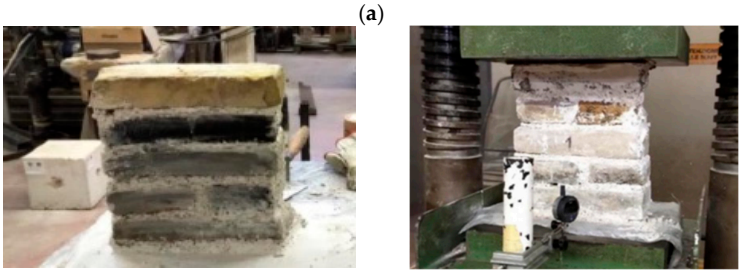

(**b**)

Figure 6. Uniaxial compression test on masonry prisms: (**a**) prisms P1, P2 and (**b**) prisms P4, P5.

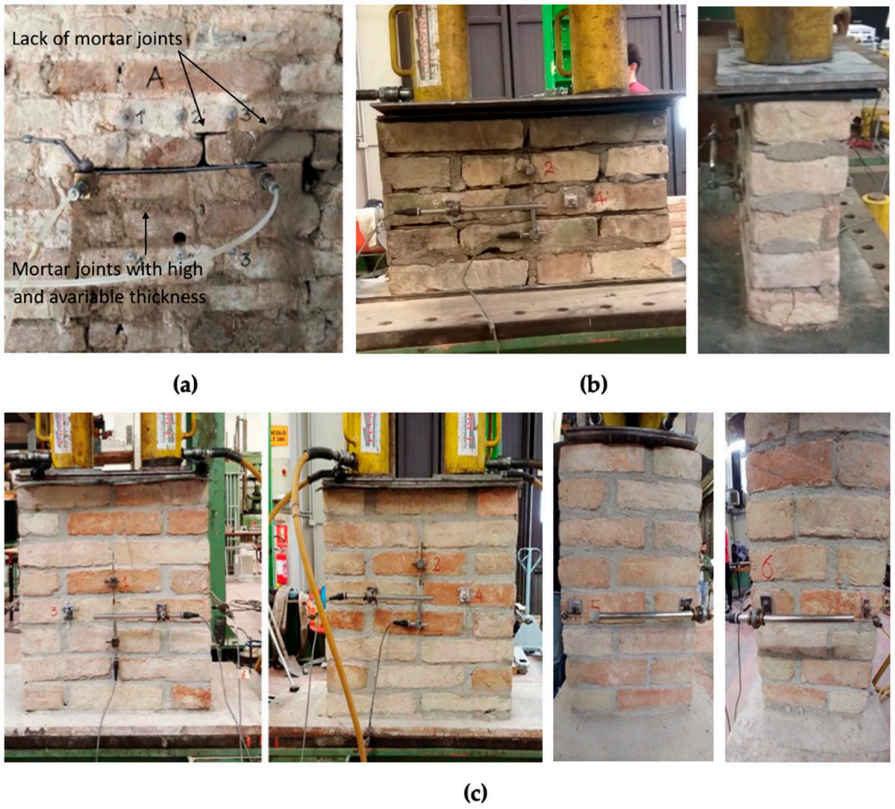

Figure 7. (**a**) Pattern of real wallette with imperfections; set-up of uniaxial compression tests on masonry wallettes (**b**) W1 and W2 and (**c**) W3.

Figure 8 illustrates the failure modes of the various panels subjected to axial compression tests. The prisms (specimens P1–P5) exhibited failure characterized by macroscopic vertical cracks, affecting both the joints and the clay bricks, accompanied by localized disintegration phenomena. The cracks developed sharply, indicating weaknesses in the mortar joints and poor adhesion between the mortar and the bricks. The failure mechanism of the specimens initiated with vertical splitting occurring shortly before the peak load was attained. In the case of specimens with 1:1:5 mortar joints, vertical fractures propagated from the edges inward, following the head joints and units, once the splitting mechanism was activated (Figure 8a). Conversely, in the specimens with weaker mortar joints, widespread cracking developed primarily in the central region, even under relatively low strain levels (Figure 8b). In the case of wallettes W1 and W2, vertical and sub-vertical cracking was observed, with noticeable detachment of the mortar in the lower courses (Figure 8c,d). The cracks appeared less defined, suggesting a progressive failure mechanism, likely attributable to the low cohesion of the mortar and the high porosity of the constituent materials. The red lines trace the propagation paths of the cracks, which typically originate at the base and develop upwards along the vertical axis. In specimen W2, localized crushing at the base of the panel was observed, indicating a differential failure in the lower joints. For the specimen W3, a misalignment of the blocks was noted, accompanied by sub-vertical cracking (Figure 8e). A prominent vertical crack was also found across the thickness of the panel, likely due to bulging effects induced by the internal core configuration of the masonry. This instability, coupled with out-of-plane displacements, closely resembles the behaviour commonly observed in historic buildings subjected to uneven thrusts.

Figure 8. Failure mode of masonry specimens under compression load: (**a**) P2 and P3; (**b**) P4; (**c**) W1; (**d**) W2 and (**e**) W3.

Figure 9 shows the results obtained in terms of the stress-strain curves for prisms P1-P5. The mechanical results of the compression tests on prisms and wallettes, in terms of peak compressive strength (f_w), vertical and horizontal strains at peak stress (ε_{vp}, ε_{hp}), chord Young's modulus ($E_{w,c}$), secant Yung's modulus ($E_{w,1/3}$) and Poisson ratio (ν_w), are summarized in Table 9.

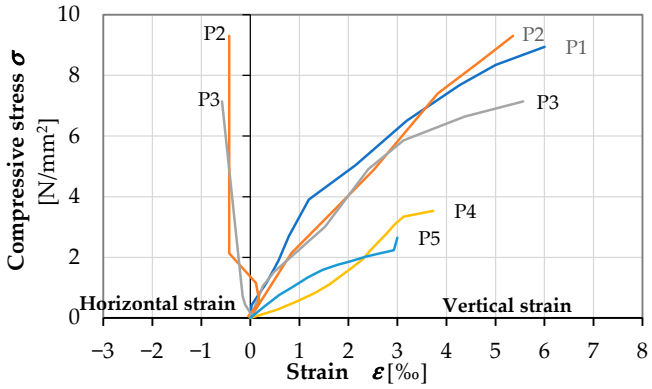

Figure 9. Stress-strain diagrams obtained from uniaxial compression load tests for prisms P1, P2, P3, P4 and P5.

Table 9. Experimental mechanical parameters of masonry (prisms and wallettes) obtained from uniaxial compression load tests.

Specimen	Mortar	f_w [N/mm²]	ε_v [‰]	ε_h [‰]	$E_{w,c}$ [N/mm²]	$E_{w,1/3}$ [N/mm²]	ν_w
P1	1:1:5	8.93	1.69	-	2961	3271	-
P2	1:1:5	9.30	7.49	0.43	2092	2500	0.14
P3	1:1:5	7.14	7.10	0.58	2037	1976	0.15
P4	1:3	3.00	2.64	-	1076	1140	-
P5	1:3	3.50	2.99	-	778	687	-
W1	1:3	1.56	2.29	0.25	981	906	0.22
W2	1:3	1.83	2.57	0.22	892	1100	0.18
W3	1:3	2.96	3.01	0.20	1752	1567	0.24

The experimental results clearly indicate that the compressive strength measured on wallettes was approximately 50% lower than that obtained from prism tests. Such a reduction has been widely documented and confirmed in the literature [48] and is generally attributed to the penalizing influence of vertical mortar joints, which significantly reduce the overall compressive capacity of masonry assemblies. For the purpose of ensuring a consistent basis for comparison and enabling a meaningful discussion of the data, the masonry compressive strength, f_w, was derived from wallette tests. These values are considered more conservative and are regarded as a more reliable representation of the actual in-situ behaviour of masonry panels. On this basis, the compressive strength of masonry made with 1:1:5 mortar was estimated by reducing the mean prism strength by 50%, obtaining an average value of approximately 4.43 N/mm². Conversely, the compressive strength of masonry with 1:3 mortar was determined directly from experimental measurements, resulting in a mean value of 1.695 N/mm². Starting from the σ-ε diagrams shown in Figure 9, different estimations of Young's modulus were determined using two approaches: the chord modulus ($E_{w,c}$), evaluated between 5% and 30% of the peak compressive strength [49]; and the secant modulus corresponding to one-third of the peak compressive strength ($E_{w,1/3}$), as defined by [30–32]. This procedure was adopted to obtain the most accurate estimate of Young's modulus, minimizing local artifacts induced by the initial lack of mechanical contrast between the masonry specimen and the testing apparatus. The compressive strength and modulus of elasticity of the tested specimens were lower than those of reference specimens constructed with a 1:1:5 mortar mix. In contrast, a higher Poisson's ratio was observed, likely due to the stress state developing within a reduced mortar layer

thickness, which contributed to increased deformability. The reduction in the mechanical properties of mortar had a direct and measurable impact on both compressive strength and elastic modulus under uniaxial compression, confirming that the mortar joints represent the primary weakness in the load-bearing behaviour of masonry under compressive stress. This high reduction in deformation capacity may be a key factor in the structural response of historical masonry and should be considered carefully in safety assessments.

Finally, two in situ tests with single and double flat jacks were carried out on the two monumental masonry buildings (Figure 10a,b) with the aim of determining the current in-service stress levels and to assess the deformation characteristics that a masonry walls may have in "real" conditions. The in-situ flat jack tests enabled the determination of the mechanical properties of the masonry, as presented in Table 10. The results obtained from these tests are consistent with those derived from the experimental tests carried out on masonry wall specimens, especially for the 1:3 cases. The differences between the two buildings can be attributed to the varying quality of construction and the differential degradation of the materials, which are also visually discernible (Figure 10).

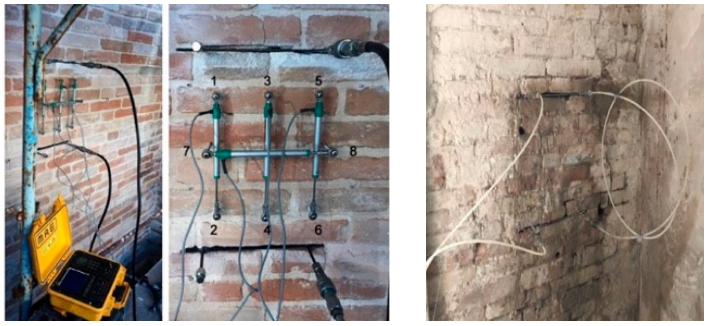

(**a**) (**b**)

Figure 10. Flat jack tests: (**a**) church of Santa Maria Ausiliatrice in Monte Ottone (MP1); (**b**) church of San Pietro in Corridonia (MP2).

Table 10. Mechanical parameters of masonry obtained from in-situ flat jack tests.

	f_w [N/mm²]	E_w [N/mm²]	v_w
MP1	3.50	2998.00	0.28
MP2	1.00	800.00	0.22

2.3. Diagonal Compression Tests on Brickwork

Diagonal compression tests to failure were performed on three wallettes, S1, S2 and S3, made of full-scale solid brick masonry of average size 300 × 130 × 50 mm (mortar 1:1:5) with side equal to about 600 mm (Figure 11). The specimens were conditioned at 20 ± 1 °C and 65 ± 8% relative humidity up to the testing age. The experimental displacements, u_h and u_v, corresponding to each load increment of specimens S1, S2, and S3 were recorded by LVDTs placed along the diagonals on both principal faces of the specimen.

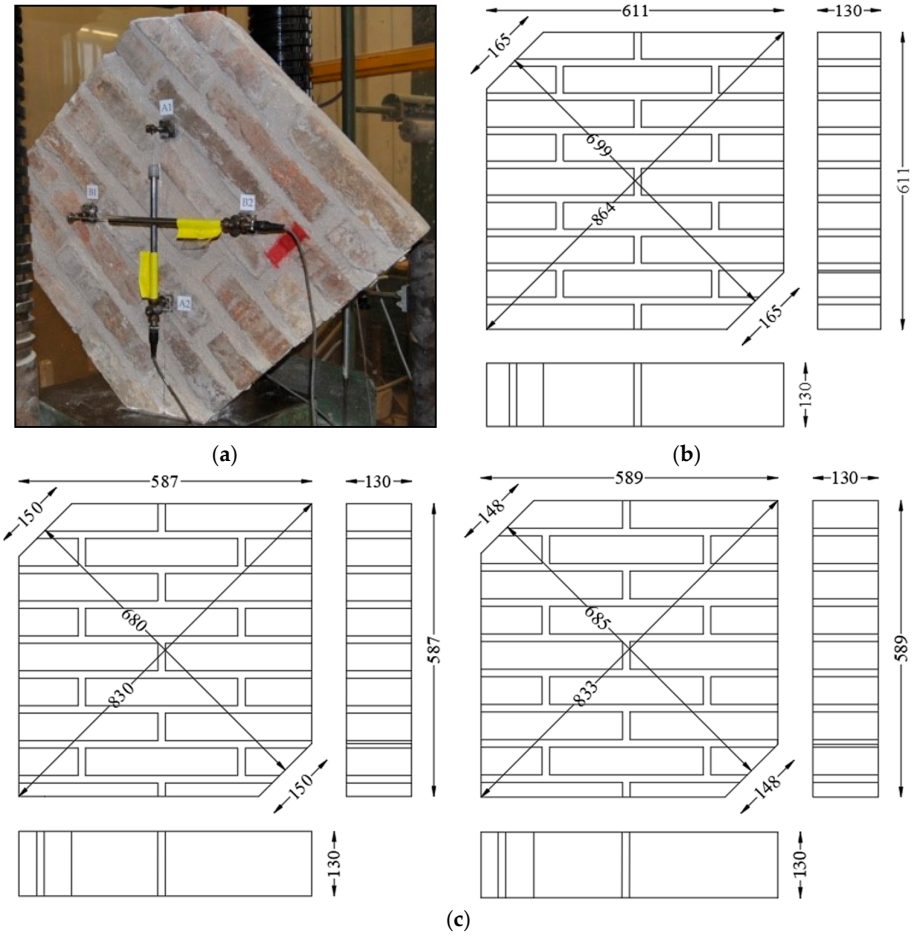

Figure 11. Wallets for diagonal compression tests: (**a**) S1, (**b**) S2, and (**c**) S3.

The outcomes of the diagonal compression tests are reported in Table 11. In this table, vertical and horizontal strains are indicated by ε_v and ε_h, respectively, while τ and γ represent the average shear stress and shear strain, evaluated in accordance with the ASTM E519–2010 standard [50]. Figure 12 presents the experimental diagrams corresponding to the diagonal compression tests conducted on specimens S1, S2, and S3. A summary of the experimental results obtained from these tests is provided in Table 12. The test was interpreted assuming a pure shear state at the panel centre, with principal stresses aligned along the diagonals. The masonry shear strength τ_u was thus computed as:

$$\tau_u = \frac{0.707 \cdot P_u}{A} \tag{2}$$

where P_u is the maximum compressive load at failure and A is the net area of the specimen.

An alternative and more realistic interpretation of the test results can be obtained by modelling the masonry panel as an isotropic and homogeneous material and performing a linear elastic analysis [51]. Based on this elastic solution and applying the failure criterion proposed by [26], the masonry shear strength τ_u was derived from the following expression:

$$\tau_u = \frac{1}{1.5} \cdot \left(\frac{0.5 \cdot P_u}{A} \right) \tag{3}$$

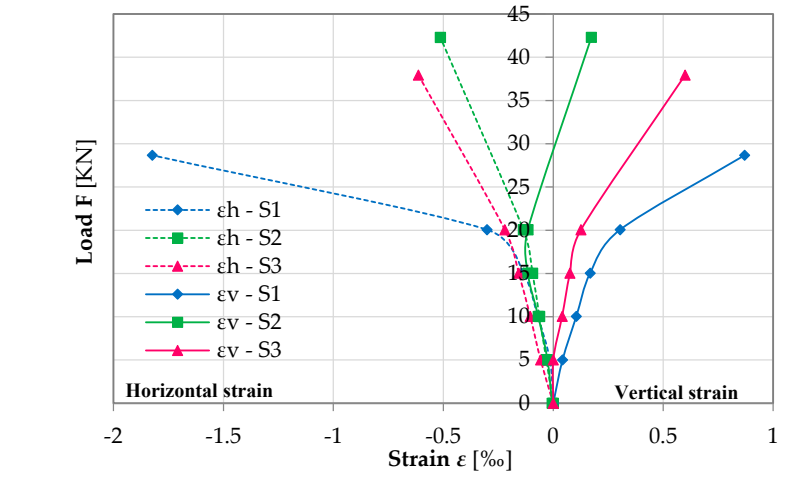

(**a**)

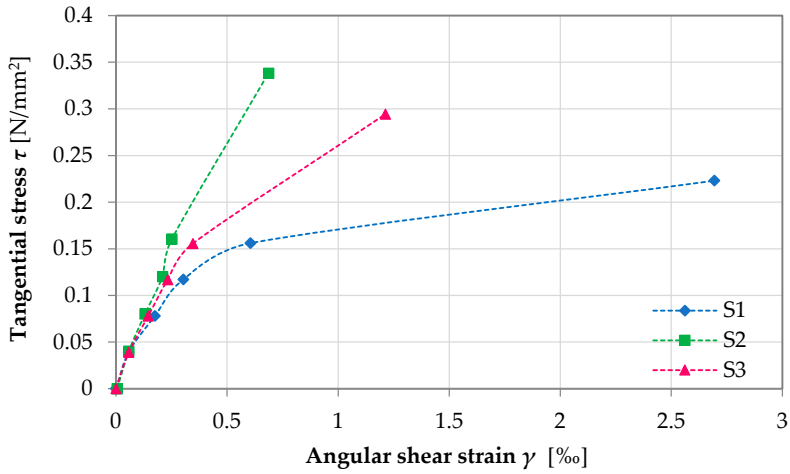

(**b**)

Figure 12. Envelope diagrams obtained from diagonal compression tests for the three wallets: (**a**) load F vs. strain ε; (**b**) stress τ vs. strain γ.

Table 11. Experimental results obtained from diagonal compression tests for S1, S2 and S3 wallettes.

S1 Wallette					S2 Wallette					S3 Wallette				
Load [N]	ε_h [‰]	ε_v [‰]	τ [N/mm²]	γ [‰]	**Load** [N]	ε_h [‰]	ε_v [‰]	τ [N/mm²]	γ [‰]	**Load** [N]	ε_h [‰]	ε_v [‰]	τ [N/mm²]	γ [‰]
0.00	0.00	0.00	0.00	0.00	0.00	0.00	−0.01	0.00	0.01	0.00	0.00	0.00	0.00	0.00
5010	−0.02	0.04	0.04	0.06	5010	−0.03	−0.03	0.04	0.06	5010	−0.06	0.00	0.04	0.06
10,030	−0.07	0.10	0.08	0.18	10,030	−0.06	−0.07	0.08	0.13	10,030	−0.10	0.04	0.08	0.15
15,040	−0.14	0.17	0.12	0.30	15,040	−0.09	−0.12	0.12	0.21	15,040	−0.16	0.08	0.12	0.23
20,060	−0.30	0.30	0.16	0.61	20,060	−0.14	−0.12	0.16	0.25	20,060	−0.22	0.13	0.16	0.35
28,670	−1.82	0.87	0.22	2.69	42,300	−0.51	0.17	0.34	0.69	37,930	−0.61	0.60	0.29	1.21
27,000	−2.01	0.87	0.21	2.88	41,530	−0.61	0.20	0.33	0.81	37,670	−0.70	0.65	0.29	1.36

Based on the diagonal compression tests conducted on the full-scale specimens S1, S2, and S3, and using the maximum load recorded for each specimen, it was also possible to estimate the tensile strength by applying Equation (1), as defined for the splitting test. In this equation, D represents the diameter of the circle inscribed within the plane of the specimen, and t denotes the specimen thickness (Table 13).

Table 12. Mechanical parameters obtained from diagonal compression tests (coefficient of variation in brackets).

Specimen	First Cracking Load F [N]	Ultimate Load F_u [N]	Ultimate Shear Strength τ_u [N/mm²]		Shear Modulus of First Cracking G' [N/mm²]	Shear Modulus G [N/mm²]
			Equation (2)	Equation (3)		
S1	15,040	28,670	0.22	0.10	385.71	81.66
S2	20,060	42,300	0.34	0.16	637.37	495.00
S3	20,060	37,930	0.29	0.14	449.56	239.02
Average	18,390 (15.78%)	36,300 (19.17%)	0.28 (21.16%)	0.13 (22.87%)	490.88 (26.67%)	271.89 (76.77%)

Table 13. Experimental tensile strength values of masonry obtained from diagonal compression tests (coefficient of variation in brackets).

Specimen	Diameter D [mm]	Thickness t [mm]	Ultimate Load F_u [N]	Tensile Strength $f_{t,w}$ [N/mm²]
S1	611	130	28,670	0.24
S2	587	130	42,300	0.35
S3	589	130	37,930	0.31
Average	-	-	36,300 (19.17%)	0.30 (18.57%)

2.4. Triplet Tests

An effective experimental approach for evaluating the shear capacity of historic masonry is the triplet test, as outlined in the RILEM recommendations [52]. This method allows for the determination of shear strength under zero normal stress conditions. In the present study, experimental results are presented for historic URM specimens tested using a custom-designed apparatus, in which two independent hydraulic jacks were employed to apply normal and shear loads, respectively, to a double-symmetric configuration (Figure 13a). Triplets were built with 1/3rd scale bricks. The triplet specimens were assembled by stacking four of these scaled bricks per sample, separated by a mortar layer approximately 5 mm thick, as illustrated in Figure 13b,c.

A total of six triplet specimens were prepared using 1:1:5 mortar, referred to as Type T triplets, incorporating both yellow and red bricks. Additionally, five triplets were constructed with 1:3 mortar, designated as Type R triplets, also using a combination of red and yellow bricks. The curing of the specimens was carried out for 28 days under controlled laboratory conditions (20 ± 1 °C; 65 ± 8% RH) until the time of testing. Shear load was applied by the jack placed vertically (Figure 13a,c) increasing at stages until failure while the pre-compression was kept constant considering three values σ_v = 0.30–0.50–0.70 N/mm². The experimental arrangement allowed an accurate measurement of the relative shear displacement along the bed joints between the vertical bricks by using a LVTD located on one side of the specimen (Figure 13b).

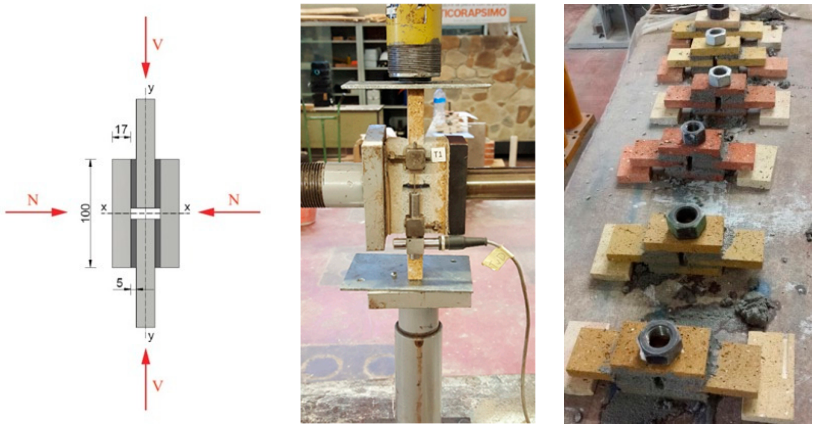

(**a**) (**b**) (**c**)

Figure 13. (**a**) Geometry of triplet in 1/3rd scale; (**b**) experimental set-up; (**c**) laboratory preparation of specimens.

The triplet tests were conducted to investigate the shear behavior of masonry under varying levels of pre-compression, with particular attention to the failure mechanisms and the role of mortar quality. At low levels of pre-compression, failure predominantly occurred at the brick–mortar interface, whereas at higher pre-compression levels, failure was frequently observed within the brick units themselves (Figure 14a). This behavior highlights the significant influence of mortar quality on the shear response of historical unreinforced masonry walls, which are often constructed using low-strength mortar. Moreover, the similarity in the failure mode of specimens made with red and yellow bricks suggests that variations in brick composition did not play a significant role in determining the failure mechanism. The main results obtained from the triplet tests are given in Figure 14b in terms of tangential stresses τ versus vertical displacement d and are summarized in Table 14. The parameters τ_0 and μ were derived from linear regression fits performed on the $\sigma_v - \tau$ scatter plots, representing the shear stress versus normal stress relationship. It should be noted that the shear strength τ_0 derived from diagonal compression tests [50] and that obtained from triplet tests [52] are not strictly equivalent. In diagonal compression, the calculated τ_0 represents an apparent shear stress corresponding to a mixed shear–tensile state acting within the masonry assemblage, whereas in triplet tests the stress field is predominantly pure shear acting along the mortar–brick interfaces. Consequently, the two parameters describe quite different mechanical aspects of the masonry behavior, and their comparison should be regarded as qualitative.

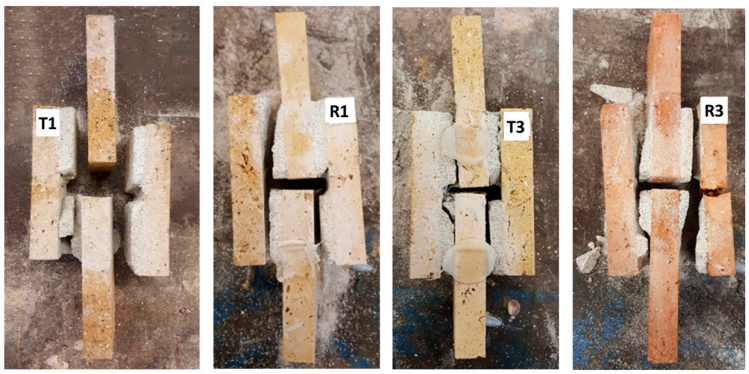

(**a**)

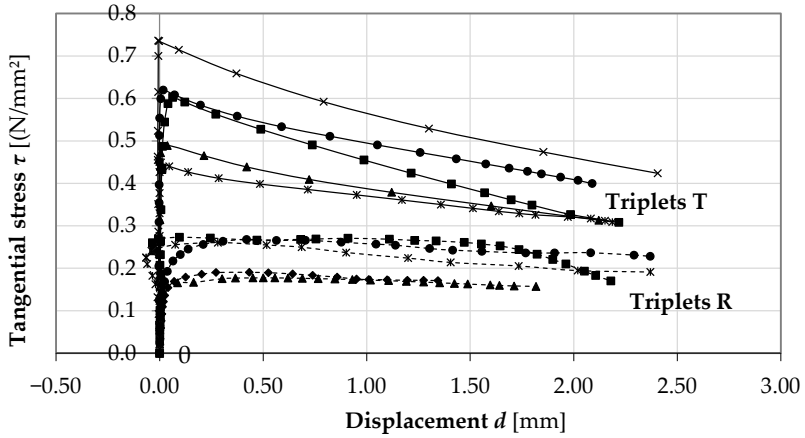

(**b**)

Figure 14. Results of triplet tests: (**a**) failure mode of triplets; (**b**) experimental diagrams tangential stress τ versus displacement recorded by LVDT.

Table 14. Experimental data obtained from triplet tests for series T and R (coefficient of variation in brackets).

	Precompression Stress σ_v	**Compression Load N**	**Specimen**	**Ultimate Tangential Stress τ_v**	**$\tau_{v,average}$**	**Cohesion τ_0**	**Friction Coefficient μ**
	[N/mm²]	[N]		[N/mm²]	[N/mm²]	[N/mm²]	
Triplets T (mortar 1:1:5)	0.30	1350.00	T1 (Y)	0.26	0.37 (40.7%)	0.15	0.76
		1350.00	T2®	0.47			
	0.50	2250.00	T3 (Y)	0.59	0.51 (22.16%)		
		2250.00	®(R)	0.43			
	0.70	3150.00	T5 (Y)	0.60	0.67 (14.78%)		
		3150.00	T6 (R)	0.74			
Triplets R (mortar 1:3)	0.30	1350.00	R1 (R)	0.19	0.185 (3.82%)	0.13	0.21
		1350.00	R2 (Y)	0.18			
	0.50	2250.00	R3 (R)	0.27	0.265 (2.67%)		
		2250.00	R4 (Y)	0.26			
	0.7	3150.00	R5 (R)	0.26	0.26		

2.5. Summary of Experimental Tests

A comprehensive summary of the entire experimental campaign is presented in Table 15. A close correspondence is observed between the outcomes of the experimental compression tests and those obtained from the semi-destructive in-situ investigations. This is especially evident in the case of wallettes constructed with a 1:3 mortar ratio, which exhibit behaviour consistent with in-situ measurements on masonry built with lower-quality materials. This consistency confirms the appropriateness of adopting a 1:3 mortar mix for the laboratory replication of severely degraded masonry.

A broader comparison between the laboratory destructive tests and the in-situ flat-jack measurements highlights the differences in mechanical behavior between idealized specimens and real construction materials. Overall, laboratory tests yielded higher mechanical parameters due to controlled materials and boundary conditions. In contrast, in-situ flat-jack tests provided lower values, representative of the actual state of the masonry. The comparison highlights that laboratory tests define the upper-bound

mechanical properties of masonry, whereas in-situ results capture the effects of aging, irregular bonding, and material decay. The integration of both datasets is thus crucial for obtaining realistic mechanical parameters for numerical modelling and structural assessment of historic masonry.

Table 15. Summary of experimental campaign results (coefficient of variation in brackets).

	f_w [N/mm²]	f_{wt} [N/mm²]	E_w [N/mm²]	G [N/mm²]	τ_0 [N/mm²]	μ
Laboratory destructive tests						
Masonry with 1:1:5 mortar	4.43 (13.6%)	0.3 (18.6%)	2363 (21.9%)	490.88 (26.65%)	0.15	0.76
Masonry with 1:3 mortar	1.7 (11.3%)	-	936.5 (6.7%)	-	0.13	0.21
In situ tests						
Masonry with good quality materials	3.50	-	2998	-	-	-
Masonry with degraded materials	1.00	-	800	-	-	-

A comparison between the experimental results and the mechanical values provided in the Italian Technical Code [30] (Table 16) reveals a satisfactory level of consistency, particularly when accounting for the reduction factors prescribed by the code for masonry with thicknesses exceeding 13 mm—namely, reduction coefficients equal to 0.7 for strength parameters and 0.8 for elastic moduli.

Table 16. Table C8.5.I of Italian Technical Code [30] about reference values for mechanical parameters of historic masonry.

Type of Masonry	f_w [N/mm²]	τ_0 [N/mm²]	E [N/mm²]	G [N/mm²]	w [kN/m³]
	Min-Max	Min-Max	Min-Max	Min-Max	
Caotic stone masonry (pebbles, erratic and irregular stones)	1	0.018	690	230	19
	2	0.032	1050	350	
Masonry with rough-hewn ashlars, with leaf of limited thickness and internal core	2	0.035	1020	340	20
		0.051	1440	480	
Split stone masonry with good texture	2.60	0.056	1500	500	21
	3.80	0.074	1980	660	
Irregular masonry made of soft stone (tuff, calcarenite, etc.)	1.4	0.028	900	300	13
	2.2	0.042	1260	420	16
Masonry made of regular blocks of soft stone (tuff, calcarenite, etc.)	2.0	0.04	1200	400	13
	3.2	0.08	1620	500	16
Masonry made of squared stone blocks	5.8	0.09	2400	800	13
	8.2	0.12	3300	1100	16
Masonry with solid clay brick and lime mortar	2.6	0.05	1200	400	18
	4.3	0.13	1800	600	
Masonry with semi-perforated clay block with cement mortar (e.g.: double UNI volume of holes ≤ 40%)	5.0	0.08	3500	875	15
	8.0	0.17	5600	1400	

3. Finite Element Modelling Analysis

In parallel with the experimental campaign, a numerical investigation of the Church of Santa Maria Ausiliatrice (Figure 2a), located in Montottone (FM), Central Italy, was performed through finite element modelling (FEM). The building, which served as the source of materials for the experimental programme, has suffered severe damage during the 1997 and 2016–2017 Central Italy seismic sequences, further aggravated by environmental degradation. The numerical study aimed to gain deeper insight into the

stress distribution and deformation behaviour of the structure under horizontal seismic loads.

In the field of masonry modelling, three main approaches can be identified: (i) detailed micro-modelling, where units and mortar joints are discretized separately; (ii) simplified micro-modelling, which homogenises the joints while preserving the block discretisation; and (iii) macro-modelling, which represents masonry as a homogeneous continuum with equivalent mechanical properties [53–55]. Considering the global nature of the study and the large scale of the structure, a macro-modelling approach was adopted. This strategy allows an efficient yet realistic representation of the overall structural behaviour while maintaining a manageable computational cost.

The finite element analyses were performed using the commercial software SAP2000 [56]. The church was schematised as a set of distinct macroelements identified through the observed crack pattern (Figure 15): the apse, the façade, and the two transept portions (east and west). Each macroelement was discretized using two-dimensional thick shell elements, accounting for transverse shear deformation. To simulate the mechanical interaction between the macroelements and the longitudinal spine walls, elastic springs (link elements) were introduced along the contact interfaces. These springs were assigned translational stiffness values consistent with the in-plane stiffness of the adjacent walls, thus reproducing the partial interlocking and load transfer typical of masonry connections.

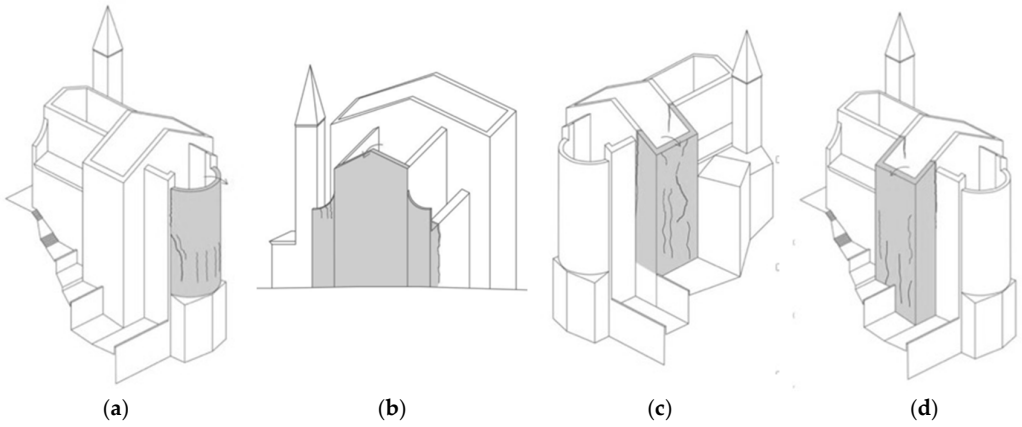

Figure 15. Cracking pattern and identification of macroelements: (**a**) apse, (**b**) façade, (**c**) east transept and (**d**) west transept.

A structured mesh with nearly regular quadrilateral elements was adopted, with an average element size of approximately 25–30 cm, ensuring adequate resolution of local stress gradients. Each of the four models contained, on average, around 45,000 nodes and 42,000 shell elements. The material parameters were assigned based on the experimental results obtained from wallettes (mortar 1:3), assuming an elastic modulus E_w = 936.5 N/mm², Poisson's ratio ν_w = 0.23 and unit weight γ = 18.5 kN/m³. These values correspond to the average mechanical properties measured during the experimental campaign on masonry specimens extracted from the same building, ensuring direct consistency between the tested material and the numerical model. Given the global nature of the study, the parameters were used as homogenized properties representative of the overall masonry behaviour. The homogenized material parameters adopted in the macro-model were directly derived from the experimental results on wallettes (Table 15), without further calibration. The objective of the FEM analysis was therefore interpretative rather than predictive, namely to assess the compatibility between the simulated stress distribution and the observed crack patterns.

Accordingly, a linear elastic constitutive model was adopted, allowing the evaluation of stress concentrations associated with the observed cracking patterns. The boundary conditions were defined to reproduce realistic support constraints: the base nodes were fully restrained in the vertical and in-plane horizontal directions, while rotational degrees of freedom were released to permit possible rocking behaviour. The contact between adjacent macroelements was modelled through shared nodes and elastic links to ensure displacement compatibility and realistic stress transfer.

A linear static seismic analysis was then performed, adopting three different levels of seismic actions:

- Seismic 10%—the seismic action applied at a given point corresponds to 10% of the dead and super dead loads acting at that point;
- Seismic NTC—the magnitude of the forces is derived from the ordinate of the design spectrum corresponding to the fundamental period T1, while their distribution over the structure follows the shape of the fundamental vibration mode in the considered direction, following the procedure given by the Italian Technical Code [30,31];
- Seismic 30 October 2016—the magnitude of the forces is determined as in the previous case, but using the ordinate of the design spectrum obtained from the elastic spectrum of the 30 October 2016 earthquake recorded in Norcia. In this case, the spectral acceleration corresponding to the fundamental period of the structure was extracted from the recorded ground motion and used to define the equivalent static horizontal loads distributed along the height of the structure with a constant vertical step; the corresponding spectral ordinates were adopted to maintain consistency with the linear elastic framework and to enable a direct comparison with the design spectrum of the Seismic NTC case.

This modelling approach enabled a consistent evaluation of the internal stress state under realistic seismic demand, while preserving computational efficiency. Although vertical and oblique cracking observed in the church may suggest local out-of-plane mechanisms or partial loss of core integrity, the present numerical investigation was intentionally limited to the in-plane behaviour of the main macroelements.

For this purpose, FE modelling thus provided insight into the in-plane stress distribution across the structural macroelements, allowing the interpretation of the observed cracking mechanisms and the assessment of stress levels with respect to the currently adopted masonry failure criteria for structural safety verification, excluding the evident cracking associated with the out-of-plane mechanisms and slenderness effects of the macroelements. Figure 16 shows the in-plane direct stresses S11 (horizontal stresses) and S22 (vertical stresses), computed with reference to the seismic event of 30 October 2016.

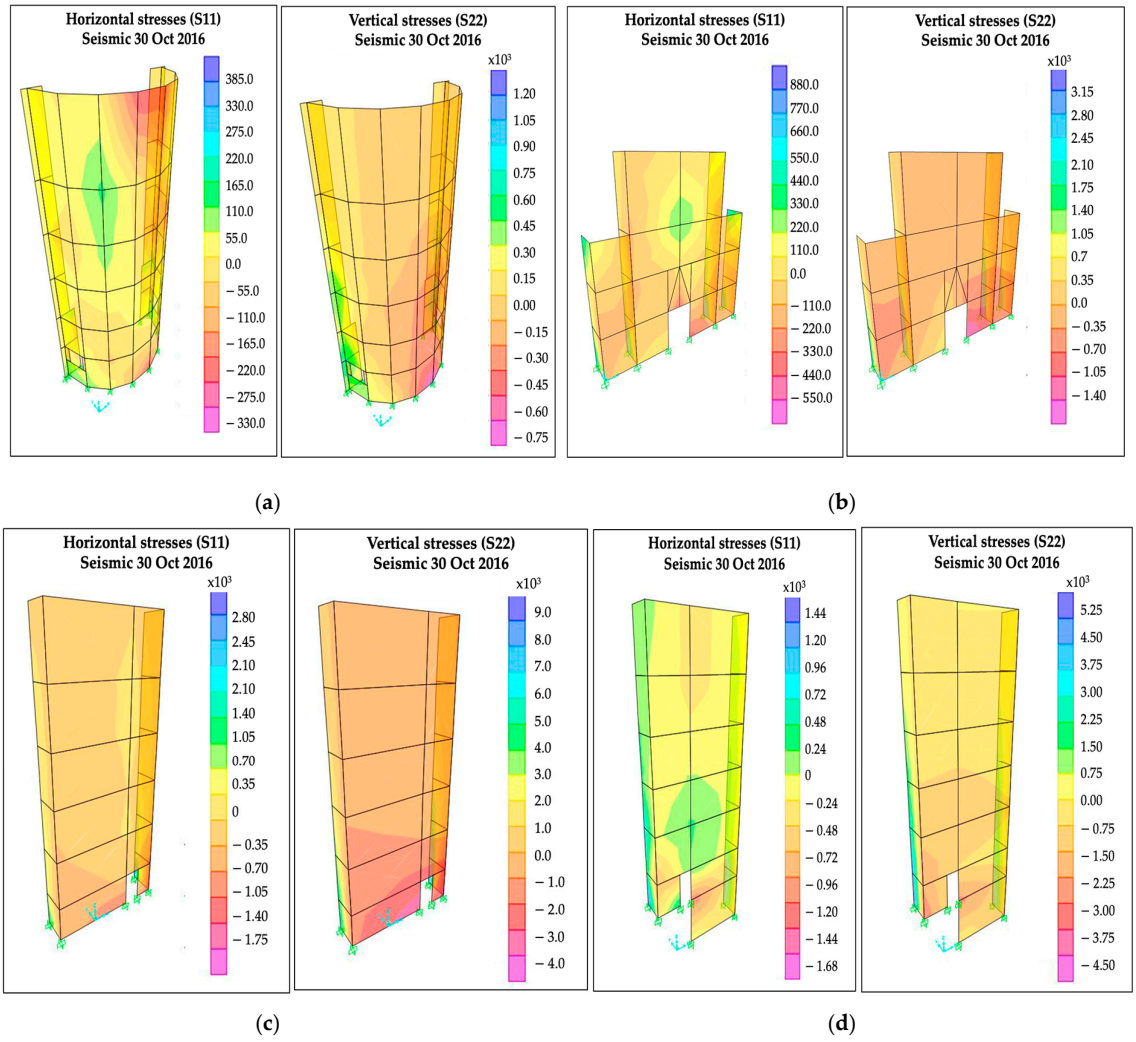

Figure 16. In plane direct horizontal stresses (S11) and vertical stresses (S22) obtained by FEM for (**a**) apse, (**b**) façade, (**c**) east transept and (**d**) west transept [units kN/m^2].

4. Discussion on Failure Mechanisms

A thorough understanding of the failure criteria of masonry is essential for conducting comprehensive vulnerability assessments, which enable the identification of potential weaknesses and failure modes. Such knowledge is indispensable for the informed design and implementation of effective retrofitting and strengthening interventions aimed at substantially enhancing the seismic resilience and overall structural performance of masonry constructions.

The following sections provide a comprehensive discussion of the main failure mechanisms associated with compression and shear, in light of the principal experimental findings. Special emphasis is placed on assessing the applicability of these criteria within the context of historic masonry, which is often characterized by mortar joints that are notably weak, severely deteriorated, and exhibit variable or considerable thicknesses.

4.1. Tensile and Compressive Mechanisms

The tensile strength of bricks is generally regarded as more critical than their compressive strength in the mechanical behaviour of masonry. When a compressive load is applied, both bricks and mortar undergo axial compression and simultaneously

develop transverse deformations perpendicular to the direction of the applied force. Based on this observation, several elastic and fracture models assuming ideal brittle behaviour have been developed and are well established in the literature [21]. The magnitude of both tensile and compressive stresses is influenced by the thickness of the mortar joints; consequently, instead of experiencing a uniaxial stress state, the individual masonry components—bricks and mortar—are subjected to a triaxial stress condition.

In elastic analysis models, transverse strains are governed by the Poisson's ratios of the constituent materials, which differ between bricks and mortar. In the absence of interaction, this would result in differential lateral strains. However, due to the presence of adhesion and friction at the brick–mortar interface, which generate tangential stresses, compatibility of deformation is enforced at the interface. As a result, the brick undergoes tensile strains while the mortar experiences compressive strains in the transverse direction. As demonstrated by ref. [21], the adhesive bond between brick and mortar is often uncertain and, under ultimate stress conditions in masonry, its contribution becomes negligible when compared to friction. Experimental investigations in literature on both modern [57] and historical [58] masonry have shown that the coefficient of friction, μ, at the brick–mortar interface typically satisfies $\mu \geq 0.7$. This value is consistent with the findings of the present experimental investigation for masonry with 1:1:5 mortar and historic bricks. In the case of masonry with weak 0:1:3 mortar and historic bricks, this value decreases significantly, reaching approximately 0.20.

The mechanical behaviour of mortar, especially in terms of Young's modulus and Poisson's ratio, varies considerably as a function of the mix proportions and its compressive strength. Based on linear-elastic analysis, the influence of mechanical and geometrical parameters on the compressive strength of masonry can be assessed, acknowledging that compressive failure is governed by the principal stress levels and the tensile (f_{bt}) or compressive (f_b) strength of the brick units. In the following sections, the compressive response of masonry made with historic bricks and weak mortar is examined using experimental data and analytical models that assume either perfectly brittle or linear-elastic material behaviour.

As it is well known, when a compressive load P is applied to masonry, an average normal stress, σ_x, is induced on both the brick surface area, A_b, and the mortar bed area, A_m. Within the framework of an elastic analysis of masonry under compressive loading, the stress state can be described as a multiaxial condition, characterized by radial tensile stresses in the brick units, σ_b, and compressive stresses in the mortar layers, σ_m.

In light of deformation compatibility between the mortar and the brick, it can be assumed that the mortar undergoes less lateral expansion than it would in an unconfined state. As a consequence of this confinement at the ultimate load, P_u, the brick in contact may experience a transverse stress state, leading to vertical cracking within the brick unit.

Simple equilibrium considerations, performed in the plane, can lead to the following equilibrium relation:

$$\sigma_b = \frac{t_m}{t_b}\sigma_m \tag{4}$$

The compression strength of mortar under confinement is influenced by its uniaxial compressive strength, f_m, and the confinement enhancement associated with triaxial stress conditions. Assuming a linear failure criterion for the mortar, the following expression can be formulated:

$$\sigma_m = \frac{\sigma_x - f_m,}{4.1} \tag{5}$$

Masonry under compression typically exhibits two distinct failure mechanisms, which may occur independently or concurrently: failure of the mortar and failure of the

brick units. When mortar cracking results from compressive crushing, the following equation is employed:

$$\sigma_b = \alpha'(\sigma_x - f_m) \qquad \alpha' = \left(\frac{\alpha}{4.1}\right), \alpha = \frac{t_m}{t_b} \tag{6}$$

In circumstances where brick cracking occurs, the unit loses its load-bearing capacity when the combined compressive–tensile stress state reaches the boundary of the brick's strength domain, corresponding to the failure condition defined by the following equation:

$$\sigma_b = f_{bt}\left(1 - \frac{\sigma_x}{f_b}\right) \tag{7}$$

In the case of simultaneous cracking of the mortar and brick, the following equation [21] is obtained:

$$f_w = \frac{f_{bt} + \alpha' f_m}{f_{bt} + \alpha' f_b} \cdot f_b \tag{8}$$

This formula enables the assessment of the compressive strength of masonry, denoted as $f_w = \frac{P_u}{A_b}$, based on the mechanical properties of its constituent materials. It is important to emphasize that the proper application of Equation (8) necessitates the inclusion of an empirical reduction factor of 1.3 which accounts for uniformity considerations related to construction quality, as well as the compressive strength of both the mortar and the bricks [21].

By examining the behavioural mechanisms of masonry through compatibility conditions, it is possible to derive additional expressions that characterize its failure response under compressive loads, taking into account the Young's moduli and Poisson's ratios of the constituent materials. If the mortar and brick are free to expand, the lateral deformations would be respectively: $\nu_m \cdot \sigma_x/E_m$ and $\nu_b \cdot \sigma_x/E_b$.

However, due to the constraint against free expansion, it is necessary—by virtue of compatibility—that their deformations conform to that of the composite masonry, expressed as $\nu_w \cdot \sigma_x/E_w$. It is well established that, under these conditions, the brick is subjected to transverse tensile stresses, while the mortar experiences transverse compressive stresses. By employing the compatibility conditions:

$$\nu_w \cdot \frac{\sigma_x}{E_w} - \nu_b \cdot \frac{\sigma_x}{E_b} = \frac{\sigma_b}{E_b} \tag{9}$$

$$\nu_m \cdot \frac{\sigma_x}{E_m} - \nu_w \cdot \frac{\sigma_x}{E_w} = \frac{\sigma_m}{E_m} \tag{10}$$

in conjunction with the equilibrium expression given in Equation (4), and assuming the mechanical properties ν_m, E_m, ν_b, E_b, t_m and t_b are known, the shear stress may be rigorously determined through the application of Equations (9)–(11).

$$\sigma_b = \frac{\upsilon_m \cdot E_b - \upsilon_b \cdot E_m}{E_m + \beta \cdot E_b} \cdot \sigma_x \tag{11}$$

with $\beta = t_b/t_m$. Given β coefficient and the Poisson's coefficient of the masonry, ν_w, an additional relationship can be derived that links σ_x and σ_b:

$$\sigma_b = k \cdot \sigma_x \tag{12}$$

with the following non-dimensional coefficient:

$$k = \frac{t_m}{t_b} \cdot \left(\upsilon_m - E_m \cdot \frac{\upsilon_w}{E_w}\right) \tag{13}$$

If $\sigma_b \geq f_{t,b}$, where $f_{t,b}$ is the tensile strength of the brick, the brick will be cracked with loss of masonry strength.

The ultimate compressive strength of the brick can be correlated with the normal compressive stress acting on the masonry, σ_x, by referring to the principal stress σ_{II} as defined by Mohr's circle, under the assumption of a plane stress condition. In this context, the tangential stress at the brick interface is assumed to arise solely from frictional resistance, with adhesion effects being neglected, such that $\tau \cong \emptyset \cdot \sigma_x$, where $\emptyset$ is taken as 0.7. Accordingly, the following relationship is established:

$$\sigma_{II} = \frac{\sigma_x - \sigma_b}{2} + \sqrt{\left(\frac{\sigma_x + \sigma_b}{2}\right)^2 + (\emptyset \cdot \sigma_x)^2} \tag{14}$$

By substituting Equation (13) into Equation (14), the following dimensionless expression is derived, establishing a relationship between the maximum compressive stress in the brick and the compressive stress in the masonry as a function of the coefficient k:

$$\frac{\sigma_{II}}{\sigma_x} = \frac{1 - k}{2} + \sqrt{\left(\frac{1 + k}{2}\right)^2 + \emptyset^2} \tag{15}$$

Therefore, by knowing the coefficient k and the maximum compressive strength of the brick $f_b = \sigma_{II}$, it is possible to determine the maximum compressive stress in masonry, f_w, associated with brick's compressive failure. Analogously, by equating the tensile strength of the brick to the principal stress $f_{bt} = \sigma_I$, it is possible to estimate the value of the stress on the masonry $\sigma_x = f_w$, that may induce brick's failure by tensile cracking. This is achieved by evaluating the ratio between the brick's tensile strength, represented by the principal stress σ_I, and the compressive stress acting on the masonry:

$$\frac{\sigma_I}{\sigma_x} = \frac{k - 1}{2} + \sqrt{\left(\frac{1 + k}{2}\right)^2 + \emptyset^2} \tag{16}$$

Given the coefficient k, the failure mechanism of the masonry can be determined by identifying the minimum stress value σ_x using Equations (15) and (16), with reference to the diagrams presented in Figure 17, where regions A and B correspond to the tensile and compressive strength domains of the brick, respectively.

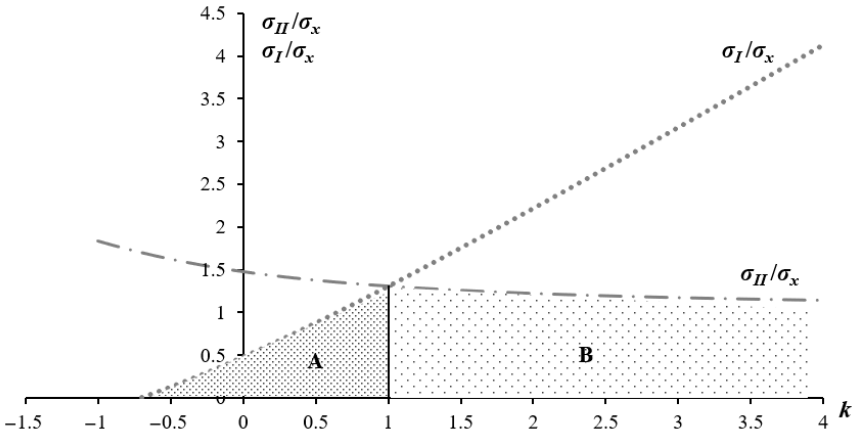

Figure 17. Diagrams of relationship between principal compressive, σ_{II}, and tensile stresses, σ_I, on the brick and masonry stress, σ_x, as a function of k coefficient.

The compressive strength of a masonry prism can also be quantitatively estimated through strain compatibility. Considering positive values for tensile strains and negative

values for compressive strains, the extensional strains in the block and masonry, denoted as ε_b and ε_m respectively, along the x and z directions, can be assessed as follows:

$$\varepsilon_{yb} = \frac{1}{E_b}\sigma_{yb} + \nu_b\frac{\sigma_x}{E_b} - \nu_b\frac{\sigma_{zb}}{E_b};\ \varepsilon_{zb} = \frac{1}{E_b}\sigma_{zb} + \nu_b\frac{\sigma_x}{E_b} - \nu_b\frac{\sigma_{yb}}{E_b} \tag{17}$$

$$\varepsilon_{ym} = -\frac{1}{E_m}\sigma_{ym} + \nu_m\frac{\sigma_x}{E_m} + \nu_m\frac{\sigma_{zm}}{E_m};\ \varepsilon_{zm} = -\frac{1}{E_m}\sigma_{zm} + \nu_m\frac{\sigma_x}{E_b} + \nu_m\frac{\sigma_{ym}}{E_m} \tag{18}$$

By compatibility, the lateral strain in the bricks and mortar are the same. By equilibrium, the total lateral tensile force on the brick must be equal to the compressive force in the mortar:

$$\sigma_{yb}\cdot t_b = \sigma_{ym}\cdot t_m;\ \sigma_{zb}\cdot t_b = \sigma_{zm}\cdot t_m \tag{19}$$

By setting $\varepsilon_{yb} = \varepsilon_{ym}$ and applying the equilibrium relations (19) the following expression can be derived:

$$\sigma_{yb} = \sigma_{zb} = \frac{\sigma_x(\phi\nu_m - \nu_b)}{1 + \alpha\phi - \nu_b - \beta\phi\nu_m} \tag{20}$$

with $\beta = t_b/t_m;\ \alpha = t_m/t_b$ and $\phi = E_b/E_m$. Neglecting the term σ_z,the following would be obtained:

$$\varepsilon_b = \frac{1}{E_b}\sigma_b + \nu_b\frac{\sigma_x}{E_b};\ \varepsilon_m = -\frac{1}{E_m}\sigma_m + \nu_m\frac{\sigma_x}{E_m} \tag{21}$$

By equilibrium assumptions, it follows that:

$$\sigma_m = \frac{t_b}{t_m}\cdot\sigma_b \tag{22}$$

By compatibility, setting $\varepsilon_b = \varepsilon_m$ and employing the equilibrium relation (22) the following expression can be derived:

$$\sigma_b = \frac{(\nu_m E_b - \nu_b E_m)}{E_m + \beta E_b}\cdot\sigma_x \tag{23}$$

This equation is analogous to Equation (11). Equation (20) indicates that lateral stresses lead to a reduction in the effective value of f_w, defined as the stress σ_x at which failure takes place. The limiting condition described by Equation (20) corresponds to the case in which σ_{yb} and σ_{zb} are equal to the uniaxial tensile strength of the block, f_{bt}, while σ_x is zero. Conversely, the other extreme scenario occurs when the compressive stress σ_x reaches the compressive strength of the brick, f_b, and the lateral tensile stresses are null.

Assuming Mohr's failure criterion as proposed by ref. [22], a linear interpolation between the two limiting points yields a relationship that defines the correlation between the tensile and compressive stresses in the block as follows:

$$\sigma_{xb} = \frac{1}{\omega}(f_b - f_w) \tag{24}$$

with $\omega = f_b/f_{bt}$. By substituting the above expression for σ_{xb} in Equation (20), the following relation between f_w and f_b is obtained:

$$\frac{f_w}{f_b} = \frac{1}{1 + \dfrac{\omega(\phi\nu_m - \nu_b)}{(1-\nu_b) + \beta\phi(1-\nu_m)}} \tag{25}$$

A comparison of the two methods for predicting the compressive strength of masonry prisms based on, respectively, stress consideration (Equation (8)) and strain compatibility (Equation (25)) is shown in Figure 18. The comparison is made for typical values that may characterize historic (Figure 18a,b) and modern masonry (Figure 18c). For

modern masonry, the two models provide closely aligned predictions. However, in the context of historic masonry, the outcomes produced by the two approaches exhibit significant discrepancies. Furthermore, it is evident that the model based on strain compatibility is more sensitive to variations in the mechanical properties of the mortar, a sensitivity that is not reflected in the model grounded in stress-based considerations.

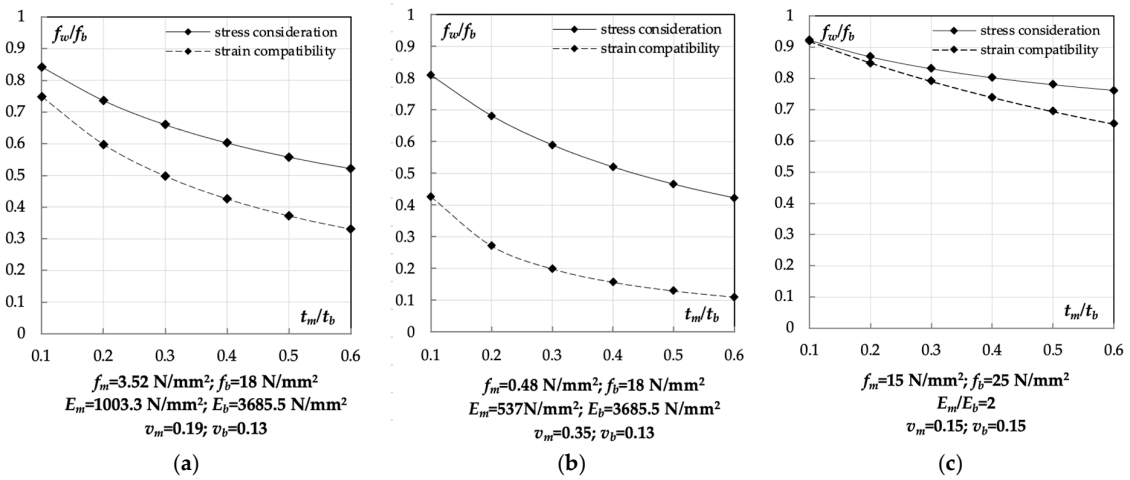

Figure 18. Relation between prism strength and thickness of components: (**a**) historic masonry with 1:1:5 mortar, (**b**) historic masonry with 1:3 mortar and (**c**) modern masonry.

Figure 19 show a comparison between experimental and analytical results obtained by stress consideration and strain compatibility, adopting as input parameters the mechanical properties of material (brick and mortar) obtained experimentally.

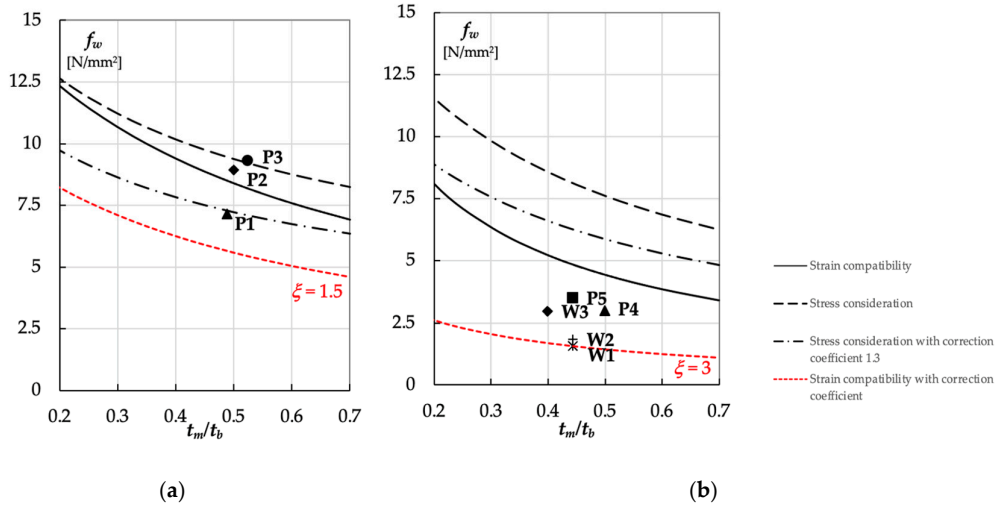

Figure 19. Comparison of analytical prediction with experimental results for (**a**) mortar 1:1:5 and (**b**) mortar 1:3 and predicted values by Codes.

In the case of historic masonry with weak mortar (1:3), the analytical curves derived from equilibrium and strain–compatibility formulations do not provide conservative estimates. The curve derived using Equation (8) significantly overestimates the compressive strength of the masonry, even when applying the reduction coefficient of 1.3. This observation may be attributed to the fact that the reduction coefficient was calibrated in ref. [21] for modern masonry constructed with cement mortars within the medium strength range.

Among the two models, the strain compatibility-based approach proves to be more effective from a predictive standpoint, although it may require the adoption of correction factor ξ to achieve a more accurate and cautelative fit to the experimental results:

$$f_w = \frac{1}{\xi}\frac{1}{1+\frac{\omega(\phi\nu_m-\nu_b)}{(1-\nu_b)+\beta\phi(1-\nu_m)}}f_b \quad (26)$$

with $\xi(f_m) = -1.44f_m + 5.58$.

In this regard, for historical masonry, it is proposed to adopt a specific adjustment for low strength mortars with a correction factor ξ ranging between 1.5 and 3, depending on the type of mortar used and its mechanical properties (Figure 19).

Guidelines for the evaluation of the compressive strength of masonry are also provided in Eurocode 6 [28] and in literature by many authors [22]. The formulation proposed by EN 1996-1-1 [59] allows for the estimation of masonry compressive strength based on the compressive strength values of its individual components, namely bricks and mortar:

$$f_w = Kf_b^{\alpha}f_m^{\beta} \quad (27)$$

in which K is a coefficient that depends on the type of masonry blocks and on the characteristics of mortar (thickness and density), α and β are constant equal to 0.7 and 0.3, respectively. Several studies in literature [60–62] suggest the recalibration of the coefficients K, α and β to better align the EN 1996-1-1 model with available experimental data. This adjustment aims to establish appropriate coefficient ranges for various types of manufactured masonry units and mortars, which are not directly applicable to the assessment of historic masonry.

The degradation to which historic masonry may be subjected calls for the necessity of recalibrating the coefficients provided by EC6 and for a possible reformulation of expression (27). Taking into account the parameters that most significantly influence the determination of mechanical strength, as well as the data that can be most readily obtained during the in-situ assessment of an existing masonry structure (such as the mechanical strength of units obtained through destructive and non-destructive methods [60] and the thickness of both mortar joints and units), the following formulation is proposed. This formulation, derived through a multiple power regression analysis, serves as a tool for evaluating the compressive strength of existing masonry in the presence of weak mortar joints.

$$f_w = 0.034f_b^{1.53}\left(\frac{t_m}{t_b}\right)^{-0.35} \quad (28)$$

As shown in Table 17, the proposed formulation demonstrates excellent agreement with the experimental data (R^2 = 0.9975, RMSE = 0.029), confirming the robustness of the adopted power-law relationship. Compared with existing analytical models, which tend to overestimate the compressive strength, the proposed equation provides predictions that are more consistent with the observed values (Table 18). Although the regression is based on a limited dataset (n = 5), the confidence interval of the second exponent is relatively wide and the potential variability in texture or bedding is not considered, the overall correlation remains strong. The proposed relationship appears particularly suitable for masonry with weak or deteriorated mortars characterized by f_m < 0.5 N/mm^2 and joint thicknesses greater than 2 cm, conditions under which conventional formulations are less reliable.

Table 17. Statistic metrics of the regression model.

Observations	R^2	Root Mean Square Error	Cross-Validation	Confidence Intervals of the Exponents
5	0.9975	0.029	- [1]	x_1: 1.24 ÷1.81 x_2: −1.05 ÷ 0.36

[1] Cross-validation was not performed due to the limited dataset size.

Table 18. Predicted and experimental masonry's compressive strength f_w.

Masonry Compressive Strength f_w [N/mm²]				
Experimental Tests	Stress Consideration (Equation (8))	Strain Compatibility (Equation (26))	Formulation EC6 (Equation (27))	Proposed Formulation (Equation (28))
3.00	5.26	4.32	3.21	3.01
3.50	6.18	4.83	3.34	3.47
1.56	4.78	4.22	2.23	1.53
1.83	5.18	4.46	2.49	1.88
2.96	6.08	4.96	3.05	2.95

4.2. Shear Mechanisms

Brick masonry walls subjected to biaxial compression and shear are generally characterized by two principal failure mechanisms: (a) cracking localized along vertical and horizontal mortar joints, primarily governed by bond shear at the onset and subsequently by frictional resistance, the magnitude of which is proportional to the applied pre-compression; (b) cracking that propagates through both mortar joints and masonry units, predominantly driven by tensile strain and/or stress development.

Extensive experimental evidence [63–65], derived from both model-scale and full-scale tests, has established that the shear strength of masonry, when describing shear failure accompanied by slip along mortar joints, conforms to the Mohr–Coulomb failure criterion, namely:

$$\tau_u = \tau_0 + \mu \cdot \sigma_v \tag{29}$$

where τ_0 denotes the bond shear strength in the absence of pre-compression and μ represents the coefficient of friction. Masonry shear strength is assumed to consist of an initial bond component between mortar and units, together with a frictional component proportional to the normal compressive stress on the bed joint. The empirical relation is valid for shear failure under pre-compression up to 2.0 N/mm² [60], but neglects stress distribution within the panel and has not been verified beyond this limit. For comparison with other studies on URM wall shear failure, Hendry [65] proposed a non-dimensional expression based on principal tensile stress:

$$\frac{\tau_u}{f_t} = \sqrt{\left(\frac{\sigma_v}{f_t} + 1\right)} \tag{30}$$

where f_t denotes the principal tensile stress and τ_u the average shear stress at failure.

A wide range of experimental results on masonry subjected to combined compression and shear were found to be consistent with the above relationship. It was further assumed that the principal tensile stress is influenced by the normal pre-compression on the bed joint and may be expressed as:

$$f_t = f_{t0} + \alpha \cdot \sigma_v \tag{31}$$

where f_{t0} is the value of f_t at zero pre-compression, equal to the ultimate shear stress τ_0 under pure shear. Substituting f_t from Equation (31) into Equation (30) yields:

$$\tau_u^2 = \tau_0^2 + \tau_0 \cdot \sigma_v + \alpha \cdot \sigma_v^2 + 2 \cdot \alpha \cdot \tau_0 \cdot \sigma_v + \alpha^2 \cdot \sigma_v^2 \quad (32)$$

Following ref. [65], the parameter α may be set equal to 0.05, thereby simplifying Equation (32) to the following form:

$$\tau_u^2 = \tau_0^2 + 1.1 \cdot \tau_0 \cdot \sigma_v + 0.053 \cdot \sigma_v^2 \quad (33)$$

Although this relationship depends on a single parameter—namely, the shear strength of masonry under pure shear conditions—accurate determination of this value necessitates experimental evaluations, like shear box or triplet tests.

The criteria expressed in Equations (29) and (30) are compared with the experimental results obtained from triplet tests and are illustrated in Figure 20. Curve "I", based on Coulomb's law, is derived using Equation (29) and the results from triplets T; curve "II" is obtained through the formula in Equation (30), utilizing the tensile strength, f_{tw}, determined from the diagonal compression tests. The straight line representing the law described by Equation (29) is shown together with the parallel line originating from the origin, corresponding to the condition in which the initial shear strength τ_0 is equal to zero. This configuration applies to cases of high vertical stresses, where adhesion can be reasonably neglected. Curve II characterizes a cracking mechanism involving both the bricks and the mortar joints. This mechanism is typical of masonry panels subjected to shear under medium to high compressive stress levels. Figure 20 illustrates the failure criterion suitable for historic masonry with weak and degraded joints through a three-phase diagram: the first segment (a–b) is a straight line governed by Equation (29); the second segment (b–c) follows Equation (30); and finally, a third straight line (c–d), where the resistance mechanism changes and the ultimate shear stress is governed by friction between brick and mortar, limited by the compressive force.

The criterion follows the well-known Coulomb failure criterion in the initial phase (a–b), and its application has proven to be appropriate for historic Italian cities affected by recent seismic events. This is due to the fact that, in general, the pre-compression stress in small, low-rise buildings is lower than σ_V = 0.5 N/mm². Furthermore, the results obtained from the triplet tests confirm that the three-phase failure criterion is suitable for describing the structural response of masonry buildings. Based on the triplet test data and adopting the intersection criterion, for vertical load values below σ_{V1} = 0.42 N/mm², failure is governed by sliding along the mortar joints, in agreement with Coulomb's criterion; within the range between σ_{V1} = 0.42 N/mm² and σ_{V2} = 0.74 N/mm², the governing mechanism shifts to diagonal cracking, consistent with the Mohr failure model.

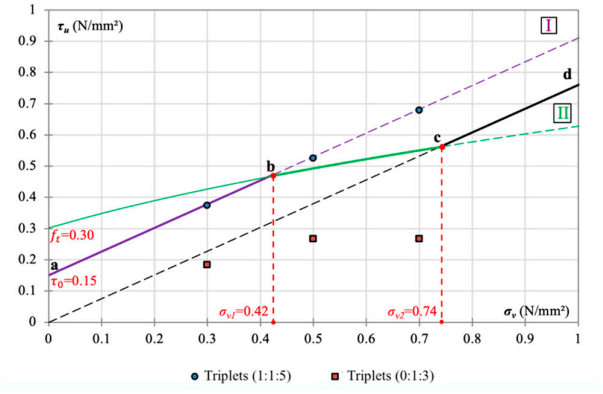

Figure 20. Experimental results of shear tests on masonry triplets compared with failure compression-shear criteria.

Finally, based on the stress values obtained through FE modelling, the stress state of each macroelement was compared with the shear strength domains derived from the failure criteria proposed by Hendry and Mohr-Coulomb (Figure 21). The comparison was performed using the maximum stresses, identified as the six highest nodal values for each macroelement under the three seismic load conditions. Analysing all the data presented in the diagrams, a minimum safety factor of γ_{min} = 1.7 and an average safety factor of γ_{av} = 5 were determined. These safety factors were evaluated as the ratio between the shear strength predicted by the Hendry and Mohr–Coulomb criteria and the corresponding maximum stress values obtained from the FE model for each macroelement. These values suggest that, with respect to shear, the macroelements exhibit high levels of structural safety. This observation supports the hypothesis that, in historic masonry buildings characterized by degraded and weak mortar joints, failure mechanisms are more likely to be governed by compressive failure. Under seismic loading, this condition may be further exacerbated when the earthquake includes not only horizontal ground accelerations but also a significant vertical component. Such combined actions increase the stress and strain demand on the materials, potentially leading to the development of vertical or near-vertical cracking patterns, as observed in the analysed case study.

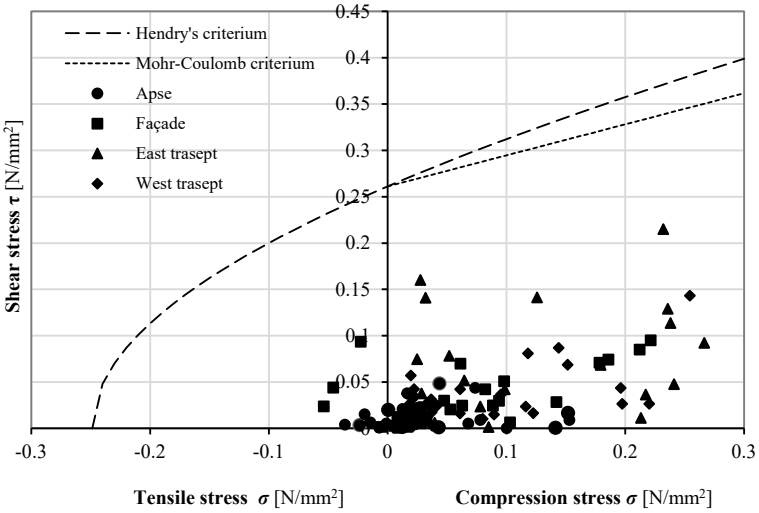

Figure 21. Comparison between stress state obtained by FEM and shear failure criteria provided by Hendry and Mohr–Coulomb.

5. Conclusions

This study examines the mechanical behaviour and failure mechanisms of historic brick masonry with weak and irregular joints through an integrated programme of experimental tests, finite element simulations and analytical models. The main outcomes are:

- Historic masonry made with low-strength lime-based mortars exhibits significantly reduced compressive and shear capacity compared to modern brickwork. Joint irregularities and poor mortar cohesion are the main contributors to its vulnerability.
- Compression tests on prisms and wallettes highlighted typical vertical splitting and cracking, confirming the brittle response of masonry with degraded mortar joints.
- Shear triplet tests indicated a three-phase failure criterion (sliding, diagonal cracking, and frictional resistance), which better represents the behaviour of historic masonry than conventional Mohr–Coulomb or Hendry formulations.

- Analytical stress- and strain-based models tend to overestimate the compressive strength of historic masonry. Corrective factors or modified formulations, as proposed in this study, are needed for realistic and conservative predictions.
- Comparison of stress states obtained by FEM with shear failure domains indicated satisfactory safety margins against shear; compressive failure and out-of-plane kinematic mechanisms remain the primary risks for masonry with weak, irregular mortar joints.
- These findings offer practical guidance for engineers and conservation practitioners involved in the assessment and strengthening of historic unreinforced masonry (URM) buildings. The experimentally validated adjustments to classical failure criteria provide more reliable parameters for safety evaluations, while the combined use of laboratory tests, in-situ measurements, and numerical simulations enables a more accurate characterization of mechanical properties and failure mechanisms. This knowledge supports targeted retrofitting solutions—such as mortar joint improvement, compatible grouting, and reinforcement of critical wall connections—aimed at enhancing seismic performance while preserving architectural authenticity.
- Although the FEM modelling approach adopts linear-elastic assumptions and therefore represents a simplification of the structural response, it is consistent with strategies commonly employed in professional practice for large-scale seismic assessment. Moreover, the restricted size of the experimental dataset reflects the limited availability of historic materials. Nonetheless, the integrated experimental–numerical framework establishes a robust foundation for future advancements. Ongoing research will extend the investigation to larger-scale specimens and incorporate cyclic and dynamic testing to more realistically capture seismic effects and degradation processes. These developments are expected to improve predictive seismic modelling and provide a stronger basis for the design of minimally invasive reinforcement interventions. Further efforts will also focus on validating the proposed formulation for compressive strength assessment across a broader dataset, considering material weaknesses, mortar degradation, and variability in masonry textures and bonding patterns.

Author Contributions: Conceptualization, E.M., V.N. and F.G.; methodology, E.M.; validation, E.M., V.N. and F.G.; formal analysis, E.M.; investigation, E.M.; data curation, E.M.; writing—original draft preparation, E.M.; writing—review and editing, V.N. and F.G.; supervision, F.G. All authors have read and agreed to the published version of the manuscript.

Funding: This research was supported by research funds provided by Polytechnic University of Marche.

Data Availability Statement: The original contributions presented in this study are included in the article. Further inquiries can be directed to the corresponding author.

Acknowledgments: The authors would like to express their gratitude to the students and technicians who collaborated in the development of the experimental research. The authors have reviewed and edited the output and take full responsibility for the content of this publication.

Conflicts of Interest: The authors declare no conflicts of interest.

References

1. Shabani, A.; Kioumarsi, M.; Zucconi, M. State of the art of simplified analytical methods for seismic vulnerability assessment of unreinforced masonry buildings. *Eng. Struct.* **2021**, *239*, 112280.
2. Reynau, R.; Bru, D.; Ivorra, S. Influence of masonry bonding patterns on the diagonal compressive strength of brick walls. *Eng. Fail. Anal.* **2025**, *179*, 109768.

3. Anzani, A.; Garavaglia, E.; Binda, L. Long-term damage of historic masonry: A probabilistic model. *Constr. Build. Mater.* **2009**, *23*, 713–724.
4. Borri, A.; Corradi, M.; Castori, G.; De Maria, A. A method for the analysis and classification of historic masonry. *Bull. Earthq. Eng.* **2015**, *13*, 2647–2665.
5. Saviano, F.; Parisi, F.; Lignola, G.P. Material aging effects on the in-plane lateral capacity of tuff stone masonry walls: A numerical investigation. *Mater. Struct.* **2022**, *55*, 198.
6. Meoni, A.; D'Alessandro, A.; Mattiacci, M.; García-Macías, E.; Saviano, F.; Parisi, F.; Lignola, G.P.; Ubertini, F. Structural performance assessment of full-scale masonry wall systems using operational modal analysis: Laboratory testing and numerical simulations. *Eng. Struct.* **2024**, *304*, 117663.
7. Saviano, F.; Lignola, G.P.; Parisi, F. Experimental compressive and shear behaviour of clay brick masonry with degraded joints. *Constr. Build. Mater.* **2024**, *452*, 138880.
8. De Iasio, A.; Briganti, R.; Milani, G.; Ghiassi, B. Numerical and analytical modelling of masonry walls failure under waterborne debris impacts. *Eng. Fail. Anal.* **2025**, *182*, 110070.
9. Valluzzi, M.R.; Sbrogiò, L. Vulnerability of Architectural Heritage in Seismic Areas: Constructive Aspects and Effect of Interventions. In *Cultural Landscape in Practice*; Amoruso, G., Salerno, R., Eds.; Lecture Notes in Civil Engineering; Springer: Cham, Switzerland, 2019; Volume 26.
10. Borri, A.; Corradi, M.; De Maria, A. The Failure of Masonry Walls by Disaggregation and the Masonry Quality Index. *Heritage* **2020**, *3*, 1162–1198.
11. Işik, E.; Büyüksaraç, A.; Avcil, F.; Arkan, E.; Ayd, M.C. Damage evaluation of masonry buildings during Kahramanmaraş (Türkiye) earthquakes on February 06, 2023. *Earthq. Struct.* **2023**, *25*, 209–221. https://doi.org/10.12989/eas.2023.25.3.209.
12. Işık, E.; Bilgin, H.; Avcil, F.; İzol, R.; Arkan, E.; Büyüksaraç, A.; Harirchian, E.; Hysenlliu, M. Seismic Performances of Masonry Educational Buildings during the 2023 Türkiye (Kahramanmaraş) Earthquakes. *GeoHazards* **2024**, *5*, 700–731. https://doi.org/10.3390/geohazards5030036.
13. Sisti, R.; Di Ludovico, M.; Borri, A.; Prota, A. Damage assessment and the effectiveness of prevention: The response of ordinary unreinforced masonry buildings in Norcia during the Central Italy 2016–2017 seismic sequence. *Bull. Earthq. Eng.* **2019**, *17*, 5609–5629.
14. Vlachakis, G.; Vlachaki, E.; Lourenço, P.B. Learning from failure: Damage and failure of masonry structures, after the 2017 Lesvos earthquake (Greece). *Eng. Fail. Anal.* **2020**, *113*, 104803.
15. Liberatore, D.; Doglioni, C.; AlShawa, O.; Atzori, S.; Sorrentino, L. Effects of coseismic ground vertical motion on masonry constructions damage during the 2016 Amatrice–Norcia (Central Italy) earthquakes. *Soil Dyn. Earthq. Eng.* **2019**, *120*, 423–435.
16. Haladin, I.; Bogut, M.; Lakušić, S. Analysis of Tram Traffic-Induced Vibration Influence on Earthquake Damaged Buildings. *Buildings* **2021**, *11*, 590. https://doi.org/10.3390/buildings11120590.
17. Atmaca, E.E.; Genç, A.F.; Altunişik, A.C.; Günaydin, M.; Sevim, B. Numerical Simulation of Severe Damage to a Historical Masonry Building by Soil Settlement. *Buildings* **2023**, *13*, 1973. https://doi.org/10.3390/buildings13081973.
18. Afif-Khouri, E.; Lozano-Martínez, A.; de Rego, J.I.L.; López-Gallego, B.; Forjan-Castro, R. Capillary Rise and Salt Weathering in Spain: Impacts on the Degradation of Calcareous Materials in Historic Monuments. *Buildings* **2025**, *15*, 2285. https://doi.org/10.3390/buildings15132285.
19. Vandemeulebroucke, I.; Caluwaerts, S.; Van Den Bossche, N. Factorial Study on the Impact of Climate Change on Freeze-Thaw Damage, Mould Growth and Wood Decay in Solid Masonry Walls in Brussels. *Buildings* **2021**, *11*, 134. https://doi.org/10.3390/buildings11030134.
20. Shi, Y.; Pan, Y.; Wang, S.; Zhong, W.; Cui, J. Damage assessment method of clay brick masonry load-bearing walls under intense explosions with long duration. *Eng. Fail. Anal.* **2024**, *166*, 108830.
21. Hildorf, H.K. An investigation into the failure mechanism of brick masonry loaded in axial compression. In *Designing, Engineering and Constructing with Masonry Products*; Gulf Publishing: Houston, TX, USA, 1969; pp. 34–41.
22. Sinha, B.P.; Hendry, A.W. The behaviour of brickwork in compression. *Struct. Eng.* **1966**, *44*, 399–412.
23. Anthoine, A.; Magenes, G.; Magonette, G. Shear-compression testing and analysis of brick masonry walls. In Proceedings of the 10th European Conference on Earthquake Engineering, Vienna, Austria, 28 August–2 September 1994; pp. 1657–1662.
24. Calderini, C.; Cattari, S.; Lagomarsino, S. In-plane strength of unreinforced masonry piers. *Earthq. Eng. Struct. Dyn.* **2009**, *38*, 243–267.
25. Pan, J.-L.; Shen, J.-X.; Zhong, Z.-L.; Xia, Y.; Li, X.-D.; Zhang, Y.-Q. Damage evolution and failure mechanism of masonry walls under in-plane cyclic loading. *Eng. Fail. Anal.* **2024**, *161*, 108240.
26. Medić, S.; Hrasnica, M. In-Plane Seismic Response of Unreinforced and Jacketed Masonry Walls. *Buildings* **2021**, *11*, 472. https://doi.org/10.3390/buildings11100472.

27. Magenes, G.; Calvi, M. In-plane seismic response of brick masonry walls. *Earthq. Eng. Struct. Dyn.* **1997**, *26*, 1091–1112.
28. Turnsek, Y.; Cacovic, F. Some experimental results on the strength of brick masonry walls. In Proceedings of the 2nd International Brick Masonry Conference, Stoke-on-Trent, UK, 12–15 April 1970; pp. 149–155.
29. Mann, W.; Müller, H. Failure of shear-stressed masonry. *Proc. Br. Ceram. Soc.* **1980**, *27*, 223–235.
30. *D.M. 14.01.2008*; Nuove Norme Tecniche per le Costruzioni. Ministero delle Infrastrutture e dei Trasporti: Via Giuseppe Caraci, Roma, 2008.
31. *Circolare n. 617 02.02.2019*; Istruzioni per l'Applicazione delle "Nuove Norme Tecniche per le Costruzioni". Ministero delle Infrastrutture e dei Trasporti: Rome, Italy, 2009.
32. European Committee for Standardization (CEN). *Eurocode 6: Design of Masonry Structures—Part 1-1: General Rules for Reinforced and Unreinforced Masonry Structures*; CEN: Brussels, Belgium, 2005.
33. Acito, M.; Buzzetti, M.; Chesi, C.; Magrinelli, E.; Milani, G. Failures and damages of historical masonry structures induced by 2012 northern and 2016–17 central Italy seismic sequences: Critical issues and new perspectives towards seismic prevention. *Eng. Fail. Anal.* **2023**, *149*, 107257.
34. Işık, E.; Avcil, F.; Harirchian, E.; Arkan, E.; Bilgin, H.; Özmen, H.B. Architectural Characteristics and Seismic Vulnerability Assessment of a Historical Masonry Minaret under Different Seismic Risks and Probabilities of Exceedance. *Buildings* **2022**, *12*, 1200. https://doi.org/10.3390/buildings12081200.
35. Valente, M.; Milani, G. Damage assessment and collapse investigation of three historical masonry palaces under seismic actions. *Eng. Fail. Anal.* **2019**, *98*, 10–37.
36. Chieffo, N.; Formisano, A. The Influence of Geo-Hazard Effects on the Physical Vulnerability Assessment of the Built Heritage: An Application in a District of Naples. *Buildings* **2019**, *9*, 26. https://doi.org/10.3390/buildings9010026.
37. Ceroni, F.; Pecce, M.; Sica, S.; Garofano, A. Assessment of Seismic Vulnerability of a Historical Masonry Building. *Buildings* **2012**, *2*, 332–358. https://doi.org/10.3390/buildings2030332.
38. Gara, F.; Nicoletti, V.; Arezzo, D.; Cipriani, L.; Leoni, G. Model Updating of Cultural Heritage Buildings Through Swarm Intelligence Algorithms. *Int. J. Archit. Herit.* **2023**, *19*, 259–273.
39. Arezzo, D.; Quarchioni, S.; Nicoletti, V.; Carbonari, S.; Gara, F.; Leonardo, C.; Leoni, G. SHM of historical buildings: The case study of Santa Maria in Via church in Camerino (Italy). *Procedia Struct. Integr.* **2023**, *44*, 2098–2105.
40. Sivori, D.; Ierimonti, L.; Venanzi, I.; Ubertini, F.; Cattari, S. An Equivalent Frame Digital Twin for the Seismic Monitoring of Historic Structures: A Case Study on the Consoli Palace in Gubbio, Italy. *Buildings* **2023**, *13*, 1840. https://doi.org/10.3390/buildings13071840.
41. Krentowski, J.R.; Knyziak, P.; Pawłowicz, J.A.; Gavardashvili, G. Historical masonry buildings' condition assessment by non-destructive and destructive testing. *Eng. Fail. Anal.* **2023**, *146*, 107122.
42. *EN 1052-1*; Methods of Test for Masonry—Part 1: Determination of Compressive Strength. European Committee for Standardization (CEN): Brussels, Belgium, 2001.
43. *EN 1052-3*; Methods of Test for Masonry—Part 3: Determination of Initial Shear Strength. European Committee for Standardization (CEN): Brussels, Belgium, 2007.
44. Veiga, M.R. Air lime mortars: What else do we need to know to apply them in conservation and rehabilitation works? *Constr. Build. Mater.* **2009**, *23*, 2379–2387.
45. Moropoulou, A.; Bakolas, A.; Bisbikou, K. Investigation of the technology of historic mortars. *Cem. Concr. Compos.* **2000**, *22*, 163–170.
46. Elert, K.; Rodriguez-Navarro, C.; Pardo, E.S.; Hansen, E.; Cazalla, O. Lime mortars for the conservation of historic buildings. *Stud. Conserv.* **2002**, *47*, 62–75.
47. Lourenço, P.B.; van Hees, R.; Fernandes, F.; Lubelli, B. Structural Rehabilitation of Old Buildings. In *Building Pathology and Rehabilitation*; Chapter: Characterization and Damage of Brick Masonry; Springer: Berlin/Heidelberg, Germany, 2013; Volume 2.
48. Thamboo, J.A.; Dhanasekar, M. Correlation between the performance of solid masonry prisms and wallettes under compression. *J. Build. Eng.* **2019**, *22*, 429–438.
49. *ASTM E111-04*; Standard Test Method for Young's Modulus, Tangent Modulus, and Chord Modulus. ASTM: West Conshohocken, PA, USA, 1981.
50. *ASTM E519-10*; Standard Test Method for Diagonal Tension (Shear) in Masonry Assemblages. ASTM: West Conshohocken, PA, USA, 2010.
51. Frocht, M.M. Recent advances in photoelasticity. *ASME Trans.* **1931**, *55*, 135–153.
52. RILEM TC 127-MS. Test for masonry materials and structures. *Mater. Struct.* **1996**, *29*, 459–463.

53. Lourenço, P.B. Computational Strategies for Masonry Structures. Ph.D. Thesis, Delft University of Technology, Delft, The Netherlands, 1996.
54. Gambarotta, L.; Lagomarsino, S. Damage models for the seismic response of brick masonry shear walls. *Earthq. Eng. Struct. Dyn.* **1997**, *26*, 423–439.
55. Milani, G. Simple homogenization model for the non-linear analysis of in-plane loaded masonry walls. *Comput. Struct.* **2009**, *87*, 1163–1178.
56. Computers and Structures Inc. *SAP2000 Integrated Finite Element Analysis and Design of Structures*, Version 25; Computers and Structures Inc.: Berkeley, CA, USA, 2023.
57. Hendry, A.W.; Sinha, B.P. Mechanical properties of modern masonry materials. *Proc. Inst. Civ. Eng.* **1970**, *47*, 23–30.
58. Capozucca, R. Experimental analysis of bond strength in masonry. *Constr. Build. Mater.* **2005**, *19*, 572–578.
59. *EN 1996-1-1*; Eurocode 6: Design of Masonry Structures—Part 1-1: General Rules for Reinforced and Unreinforced Masonry Structures. CEN: Brussels, Belgium, 2005.
60. Sýkora, M.; Diamantidis, D.; Holický, M.; Marková, J.; Rózsás, Á. Assessment of compressive strength of historic masonry using non-destructive and destructive techniques. *Constr. Build. Mater.* **2018**, *193*, 196–210.
61. Dymiotis, C.; Gutlederer, B.M. Allowing for uncertainties in the modelling of masonry compressive strength. *Constr. Build. Mater.* **2002**, *16*, 443–452.
62. Witzany, J.; Cejka, T.; Sykora, M.; Holicky, M. Strength assessment of historic brick masonry. *J. Civ. Eng. Manag.* **2016**, *22*, 224–233.
63. Capozucca, R. Experimental response of historic brick masonry under biaxial loading. *Constr. Build. Mater.* **2017**, *154*, 539–556.
64. Capozucca, R. Shear Behaviour of Historic Masonry Made of Clay Bricks. *Open Constr. Build. Technol. J.* **2011**, *5* (Suppl. 1-M6), 89–96.
65. Hendry, A.W. A note on the strength of brickwork in combined racking shear and compression. *Proc. Br. Ceram. Soc.* **1978**, *27*, 47–52.